CONTROL OF MARINE GAS TURBINE POWER PLANTS

M. Hanafi

Dept. of Marine Engineering and Naval Architecture, Faculty of Engineering,
Alexandria University, Alexandria, Egypt.

ABSTRACT

A linearized model for the dynamics and control of marine gas turbine power plants with heat recuperator is presented. Both the absolute and relative stability of the control loop have been investigated. All the state variables of the control system have been analyzed for both time and frequency domains specifications. A Bond Graph dynamic model of the control system is simulated as well.

NOMENCLATURE

(notations other than those stated here are defined in paper).

A	Area of power piston (m^2)
a	Exponent coefficient in compressor's equation (-)
a_1	Walking beam length portion(m)
b	Exponent coefficient in compressor's equation (-)
b_1	Walking beam length portion(m)
[B]	Input vector (5 * 1)
C	Output signal (controlled variable deviation)(-)
C′	Centrifugal force of the governor(kg_f)
$\bar{C}_2$	Gas velocity outlet of the turbine(m/s)
C_{pc}	Specific heat of compressed air=c_p(kcal/kg.k)
C_{PT}	Specific heat of combustion gases = c_p (kcal/kg.k).
d../dt	Differentiation w.r.t time (.../s)
E	Displacement of pilot valve(m)
e	Variation of displacement of pilot valve(m)
F(..)	Function of ..
F_2	Cross-sectional area at turbine exit. (m^2)
f_n(..)	Function of ..
G(S)	Forward path reduced transfer function
G	Gas mass rate of flow(kg/s)
g	Gravitational acceleration (m/s^2)
H(S)	Feedback path reduced transfer function.
I	Mass moment of inertia of the gas turbine rotor ($kg.m^2$)
$\bar{[I]}$	Unity matrix (5*5)
K_1, K_2	Arms of the centrifugal governor
[L]	Output matrix
M	The mass moved by servo-motor (kg).
m	Accumulated mass between the exit of compressor and entrance of gas turbine (kg).
M_h	Mass of the shaft of centrifugal governor (kg).
M_R	Reduced mass of the centrifugal governor (kg).
M_S	Mass of one fly weight of the centrifugal governor (kg)
$\dot{m}_c$	Air mass rate of flow through the compressor (kg/s)
$\dot{m}_{co}$	Initial steady state air mass flow rate (kg/s).
$\dot{m}_o$	Initial steady state flow for air or gas (kg/s).
$\dot{m}_T$	Gas mass rate of flow through the turbine (kg/s).
$\dot{m}_{TO}$	Initial steady state gas mass flow rate (kg/s).
N	External power load on the propeller (kcal/s).
N_o	Initial steady state external power load (kcal/s).
n	r.p.m of the controlled system.
n_k	Medium r.p.m of the system through the droop property.
n_{max}	Maximum r.p.rm of the controlled system.
n_o	Initial steady state r.p.m of the system.
0	Suffix denoting initial steady state.
p_d	Non-dimensional relative deviation in external power signal.
$\bar{[P]}$	System matrix (5 * 5).
P	Pressure in the Brayton Cycle
p′	Variation in Pressure drop across the Power Piston (kg_f/cm^2)
P_i	Initial pressure of gas entering the turbine (kg_f/cm^2).
P_f	Final pressure of gas at exit of the turbine (kg_f/cm^2).
Q	Oil Flow rate through the power piston (m^3/s)
Q_c	Centrifugal force of the governor reduced to the shaft (Kg_f)
Q_{max}	Maximum steady state centrifugal or spring force reduced to the shaft (kg_f).
Q_o	Initial steady state spring or centrifugal force of

the governor reduced of the shaft (kg_f)

Q_R Spring force of the governor reduced to the shaft (kg_f).

$\dot{Q}'$ Rate of heat released in the combustion chamber (kcal/s)

$\dot{Q}'_o$ Initial steady state rate of heat released in the combustion chamber (kcal/s)

q Specific heat transferred (kcal/kg).

$\bar{q}$ Variation in rate of oil flow to the power piston (m^3/s)

R Gas constant ($kg_f.m/kg.k$)

R' Spring force in centrifugal governor (kg_f)

S Laplace operator (1/s)

s Specific entropy in Brayton-Cycle (kcal/kg.k)

S_o Initial sleeve displacement (m).

S_l Sleeve's displacement (m).

S_{lmax} Maximum sleeve's displacement (m).

T Absolute temperature in the Brayton-Cycle (K).

T_i Initial temperature of gas entering the turbine (K)

t Time (s).

t_m Time constant of the accumulator between Compressor and gas turbine (s).

t_Θ Time constant of the gas turbine's rotor (s)

t_{DS} Time constant of the servo-motor (s).

t^2_{Mr} Square of a time constant of centrifugal governor (s^2).

t_{Dr} Time constant of the centrifugal governor (s).

U Magnification factor (-)

v Specific volume in the Brayton-cycle (m^3/kg)

v_i Initial specific volume of gas entering the turbine. (m^3/kg).

v_2 Specific volume of gas at the exit of turbine (m^3/kg).

V_h Velocity of the sleeve (m/s).

V_S Velocity of the fly balls (m/s).

X Inlet displacement to the walking beam (m).

x Variation of inlet displacement to the walking beam (m).

$[\bar{X}]$ State matrix (5*1)

Y Displacement of the power piston (m).

y Variation of displacement of the power piston (m).

α C_{PT}/C_{PC} (--)

β Frictional (damping) coefficient in governor ($kg_f.s/m$)

β' Frictional (damping) coefficient in servo motor ($kg_f.s/m$).

γ Ratio of specific heats of air = 1.4 (--)

$\Delta...$ Change in ...

δ Proportionality of the centrifugal governor (--)

ϵ Pressure reducing fraction (--).

ρ_2 Gas density at turbine exit (kg/m^3).

ζ_r Relative deviation in sleeve's displacement (--).

ζ_s Relative deviation in servo-motor displacement (--)

η_c Adiabatic efficiency of compressor(-)

η_t Adiabatic efficiency of gas turbine (--).

λ/l Governor's gain (--)

μ Factor denoting the location of fuel controller (-)

ν Relative speed deviation signal (--).

Θ Initial steady state maximum temperature ratio in gas turbine (--).

Θ_k Mass moment of inertia of one rotating arm in centrifugal governor ($kg.m^2$).

π Pressure ratio in compressor (--).

τ Relative temperature deviation signal (--).

τ' Time constant of servo-motor (s).

τ_1 Time constant of servo-motor (s).

ω Angular frequency (rad/s).

ω_k Angular speed of rotating arms of governor (rad/s).

$\bar{\omega}$ Angular speed of the gas turbine's rotor (rad/s).

$[\phi(t)]$ State transition matrix. (5*5).

INTRODUCTION

The dynamic behavior and control of gas turbines is an extraordinarily complicated problem. The complication is attributed not only to the complexity of the thermal power plant in which the gas turbine constitutes a single component, but also owing to the fact that alteration in speed due to load variation will affect the compressor pressure ratio, the amount of fuel injected, the combustion temperature,the gas mass flow through the turbine beside resulting variations in recuperator's thermal equilibrium and mass accumulation.

Varying sea loads on the propeller assume further complication in regard to the control of marine gas turbines.

The earliest available literature in this domain dates back to Kirilov [1] who mathematically analyzed the problem of regulation of steam and gas turbines in stationary thermal power plants.

Within one-half decade, additional few researches [2, 3, 4] came into appearance dealing with the dynamics and evolution of industrial control of stationary gas turbines. In what concerns the marine applications Schatborn [5] studied the dynamics of gas turbine driven ships with controllable pitch propellers. Over the past two decades, several studies [6-11]-ascribed to Rubis or to his contribution with Harper-focused on the representation, operating performance, dynamics and governing of marine gas turbines with emphasis on propeller loading variation due to sea loads.

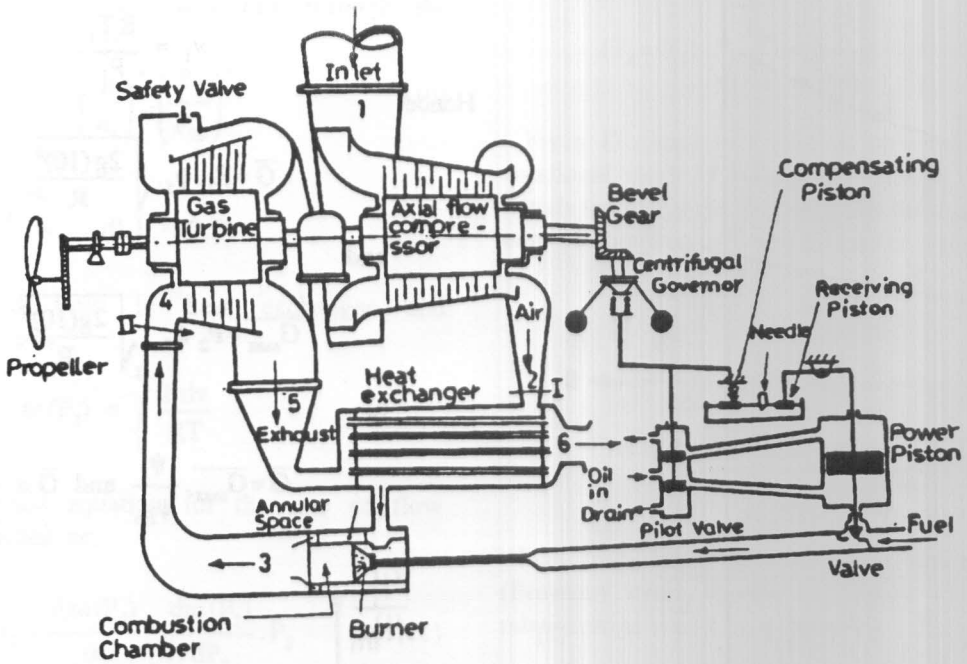

Figure 1. Marine Gas Turbine Power Plant with Recuperator and Isochronous Speed Controller.

The scope of this study will focus on the mathematical modeling of a marine gas turbine power plant with recuperator-as a heat recovery equipment,time domain analysis of the dynamics of the power plant, its dynamic behavior characteristics and frequency domain investigation of the absolute and relative stability of the control system examining its specifications. Detailed analysis of load fluctuation on the propeller due to sea loads is beyond the interest of this research, however percentage step rise (or drop) as deviation in power absorbed by the propeller in addition to sinusoidal power fluctuation as an influence of the trochoidal waves will be in practice a satisfactory assumption. A dynamic Bond Graph model of the controlled power plant is intended to be derived too.

Mathematical simulation of the dynamics of control system

Consider the marine gas turbine power plant illustrated in Figure (1). The power plant represents an axial flow air compressor-driven by the gas turbine, a heat exchanger to recuperate a portion of the heat lost with exhaust gases, a combustion chamber and the power gas turbine geared to the screw propeller. A speed control system is geared to the compressor-turbine shaft and is composed of a centrifugal speed governor attached to an isochronous (PI control property) servo motor which controls the amount of fuel passing to the burner of the combustion chamber. The Joule or Brayton gas turbine cycle is represented on both P-v and T-s coordinates Figure (2 a,b). The dotted lines shown in Figure (2 a,b) represent actual irreversible compression and expansion thermodynamic processes.

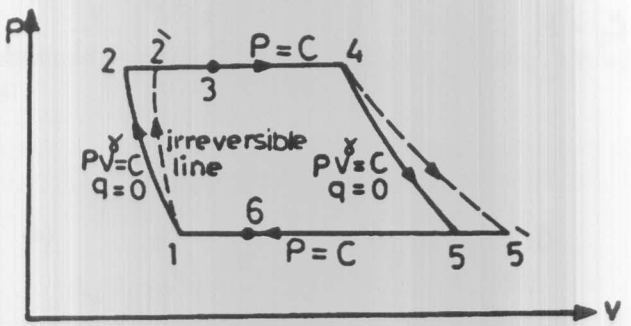

Figure 2-a. P-v Diagram of Brayton Cycle.

Considering an isentropic expansion through the turbine, the outlet gas mass rate could be written from the continuity equation (law of conservation of matter) as:

$$\overline{G} = F_2 . \overline{C_2} . \rho_2 = \frac{F_2 . \overline{C_2}}{v_2} \qquad (1)$$

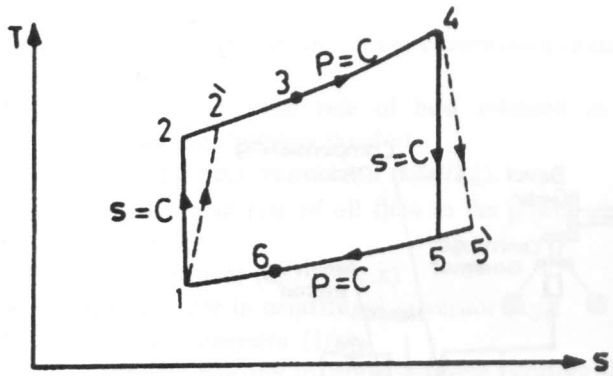

Figure 2-b. T-s Diagram of Brayton Cycle.

where the exit gas velocity C_2 [12] is:

$$\overline{C_2} = \sqrt{2g.\frac{\gamma}{\gamma-1}.10^4\, P_i V_i\left[1-\frac{P_f}{P_i}\right]^{\frac{\gamma-1}{\gamma}}} \qquad (2)$$

But

$$v_2 = \left(\frac{P_i}{P_f}\right)^{1/\gamma}.v_i \qquad (3)$$

Substituting from equations (2) and (3) into equation (1), it follows:

$$\overline{C_2} = F_2\sqrt{2g.10^4.\frac{P_i}{v_i}\left[\left(\frac{P_f}{P_i}\right)^{2/\gamma}-\left(\frac{P_f}{P_i}\right)^{\frac{\gamma+1}{\gamma}}\right].\frac{\gamma}{\gamma-1}}$$

or

$$\overline{G} = F_2\sqrt{2g\ 10^4}.\sqrt{\frac{P_i}{v_i}}.\quad \psi_f \qquad (4)$$

where:

$$\psi_f = \sqrt{\frac{\gamma}{\gamma-1}\left[\left(\frac{P_f}{P_i}\right)^{2/\gamma}-\left(\frac{P_f}{P_i}\right)^{\frac{\gamma+1}{\gamma}}\right]} \qquad (5)$$

with the assumption that combustion gases approaches in behaviour that of perfect gases, v_i could be substituted as:

$$v_i = \frac{RT_i}{P_i} \qquad (6)$$

Hence:

$$\left.\begin{aligned}\overline{G} &= F_2.\psi_f.\sqrt{\frac{2g(10)^4}{R}}.\frac{P_i}{\sqrt{T_i}}\\ \text{and}\\ \overline{G_{max}} &= F_2\,\psi_{fm}.\sqrt{\frac{2g(10)^4}{R}}.\frac{P_i}{\sqrt{T_i}}\\ \text{or}\\ \overline{G} &= \overline{G_{max}}.\frac{\psi_f}{\psi_{fm}} \text{ and } \overline{G}\,\alpha\,\frac{P_i}{\sqrt{T_i}}\end{aligned}\right\} \qquad (7)$$

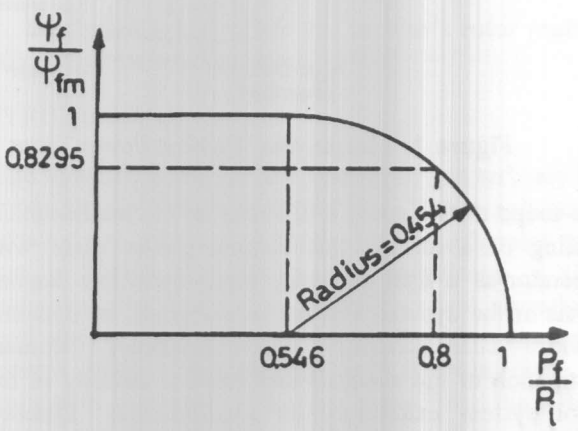

Figure 3. Pressure Ration Versus ψ Ratio.

Figure (3) demonstrates the relationship between P_f/P_i and ψ_f/ψ_{fm}. ψ_{fm} could be mathematically determined as follows:

$$\frac{d\psi_f}{d\left(\frac{P_f}{P_i}\right)}=0, \quad \text{hence } \frac{P_f}{P_i}=\left(\frac{2}{\gamma+1}\right)^{\frac{\gamma}{\gamma-1}}$$

and

$$\psi_{fm}=\sqrt{\frac{\gamma}{\gamma+1}}.\left(\frac{2}{\gamma+1}\right)^{\frac{1}{\gamma-1}} \qquad (8)$$

Let the suffix symbol "o" denote the initial steady state condition. From Figure (2) and equation (7) it could be written that:

$$\frac{\dot{m}_T}{\dot{m}_{To}}=\frac{P_4}{P_{40}}.\sqrt{\frac{T_{40}}{T_4}}\approx\frac{P_2}{P_{20}}.\sqrt{\frac{T_{40}}{T_4}} \qquad (9)$$

According to [13], the air flow rate through the compressor $\dot{m}_c = fn\,(n, P_2)$ or:

$$\frac{\dot{m}_c}{\dot{m}_{co}} = \left(\frac{n}{n_o}\right)^a \cdot \left(\frac{P_2}{P_{20}}\right)^b \qquad (10)$$

where $a \approx 1.4\text{-}2$, and

$$b \simeq -(0.1 - 0.3)$$

The accumulated flow in heat exchanger and combustion chamber is:

$$m(P_2) = \int_I^{II} \frac{P\,dv}{RT}$$

Hence the dynamic equation for the rate of flow accumulation is written as:

$$\dot{m}_c - \dot{m}_T = \frac{dm(P_2)}{dt} = \frac{dm(P_2)}{dP_2} \cdot \dot{P}_2 \qquad (11)$$

Substituting equations (9) and (10) into equation (11) yields:

$$\dot{m}_o \left[\left(\frac{n}{n_o}\right)^a \cdot \left(\frac{P_2}{P_{20}}\right)^b - \left(\frac{P_2}{P_{20}}\right) \cdot \sqrt{\frac{T_{40}}{T_4}}\right] = F(P_2) \cdot \dot{P}_2$$

or

$$\dot{P}_2 = \frac{\dot{m}_o}{F(P_2)} \left[\left(\frac{n}{n_o}\right)^a \cdot \left(\frac{P_2}{P_{20}}\right)^b - \left(\frac{P_2}{P_{20}}\right) \cdot \sqrt{\frac{T_{40}}{T_4}}\right] \qquad (12)$$

where at the initial steady state condition: $\dot{m}_{co} = \dot{m}_{To} = \dot{m}_o$. From basic thermodynamics, the rate of heat released equals the change in enthalpy during the constant pressure process 3-4, or

$$\dot{Q}' = \dot{m}_T C_{PT} (T_4 - T_3) = \dot{m}_o C_{PT} \cdot \frac{P_2}{P_{20}} \cdot \sqrt{\frac{T_{40}}{T_4}} \cdot (T_4 - T_3)$$

$$= (1 + \mu)\dot{Q}_o' \qquad (13)$$

Where μ is a non-dimensional factor depending on the position of the fuel control valve. Since:

$$\dot{Q}_o' = \dot{m}_o\, C_{PT}\, (T_{40} - T_{30})$$

equation (13) could be reduced to:

$$(T_4 - T_3) \cdot \sqrt{\frac{T_{40}}{T_4}} = (1 + \mu)\left(\frac{P_{20}}{P_2}\right)(T_{40} - T_{30}) \qquad (14)$$

From D'Alembert's rule or Newton's second law of rotational motion, the rate of change of kinetic energy equals the difference between the turbine's power and the sum of compressor's and propeller powers, i.e.

$$I \frac{d\left(\frac{\overline{\omega^2}}{2}\right)}{dt} = \dot{m}_T \cdot C_{PT} \cdot T_4 \cdot \psi_e \left(\frac{P_4}{P_5}\right) \cdot \eta_t - \frac{\dot{m}_c \cdot C_{pc} \cdot T_1 \cdot \psi_c}{\eta_c} \cdot \left(\frac{P_2}{P_1}\right) - N \qquad (15)$$

where from basic thermodynamic analysis of the Joule (Brayton) cycle shown in Figure (2), the following relationships could be deduced:

$$\pi = \frac{P_2}{P_1}, \quad \psi_c = \pi^{\frac{\gamma - 1}{\gamma}} - 1$$

$$\psi_t = \frac{P_4}{P_5} = (1 - \epsilon)\frac{P_2}{P_1} = (1 - \epsilon)\,\pi,$$

$$\psi_e = 1 - \left[\frac{1}{(1 - \epsilon)\,\pi}\right]^{\frac{\gamma - 1}{\gamma}}$$

Substituting equations (9) and (10) into equation (15) we get:

$$I \cdot \overline{\omega} \cdot \dot{\overline{\omega}} = I\overline{\omega_o^2}\left(\frac{n}{n_o}\right) \cdot \frac{d}{dt}\left(\frac{n}{n_o}\right) =$$

$$\dot{m}_o C_{pc}\left[\alpha \cdot \psi_e \left(\frac{P_4}{P_5}\right) \cdot \eta_t \cdot T_4 \cdot \left(\frac{P_2}{P_{20}}\right) \cdot \sqrt{\frac{T_{40}}{T_4}} - \frac{T_1 \cdot \psi_c}{\eta_c}\left(\frac{P_2}{P_1}\right)\left(\frac{n}{n_o}\right)^a \cdot \left(\frac{P_2}{P_{20}}\right)^b - N \right. \qquad (16)$$

where

$$\alpha = \frac{C_{PT}}{C_{PC}} \approx 1$$

Equations (12), (14) and (16) describe the dynamics of

the plant. In what concerns the governing system consider first the dynamic forces and steady state performance of a (P_2 control property centrifugal governor as illustrated in Figure (4 a,b).

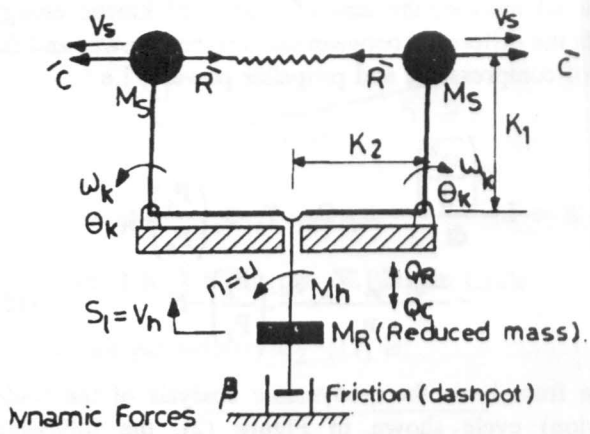

Figure 4-a. Dynamic Forces on Centrifugal governor.

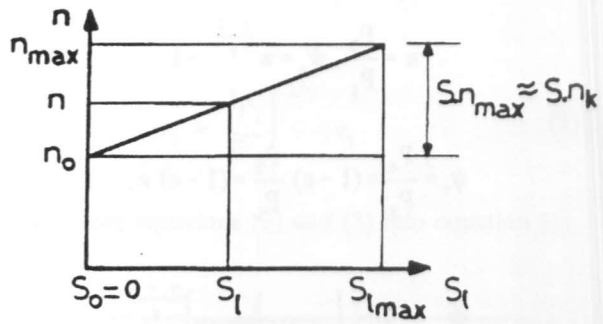

Figure 4-b. Steady State Performance of Proportional Governor (Droop Characteristic).

All masses are reduced to the shaft [14] in such a manner that the total kinetic energy of the fly weights, rotating levers and governor's shaft are kept the same fulfilling the first law of thermodynamics namely the law of conservation of energy. Hence the following equations could be written:

$$M_R = 2\left[\frac{M_h}{2} + \frac{2\theta_k}{2}\left(\frac{\omega_k}{V_h}\right)^2 + 2M_s\left(\frac{V_s}{V_h}\right)^2\right]$$

$$= \frac{\text{total K.E.}}{\left(\frac{V_h^2}{2}\right)} \qquad (17)$$

But:

$$Q_R = 2R`\frac{K_1}{K_2} \text{ and } Q_c = 2C`\frac{K_1}{K_2}$$

where Q_R and Q_c are the spring and centrifugal reduced to the governor's shaft respectively.
Also:

$$\frac{Q_c}{Q_o} = \frac{n^2}{n_o^2} = \left(\frac{n_o + \Delta n}{n_o}\right)^2 = 1 + 2\frac{\Delta n}{n_o} = 1 + 2\nu$$

where

$$\nu = \frac{\Delta n}{n_o} \approx \frac{\Delta n}{n_k}$$

If δ is defined as the proportionality of the centr governor and lies in the range of 4-5% then:

$$\delta = \frac{n_{max} - n_o}{n_{max}} \approx \frac{\Delta n_{max}}{n_o}$$

From equations (19) and (20) the maximum stead centrifugal or spring force is:

$$Q_{max} = Q_o\left\{1 + \frac{2\Delta n_{max}}{n_o}\right\} = Q_o(1 + 2\delta)$$

But:

$$\frac{Q_R - Q_o}{Q_{max} - Q_o} = \frac{S_l - S_o}{S_{lmax} - S_o} = \frac{S_l}{S_{lmax}} = \zeta_r$$

Substituting from equation (21) into equation follows that:

$$\frac{Q_R}{Q_o} = 1 + 2\delta . \zeta_r$$

Hence, the net dynamic force reduced to the sha affecting the motion of sleeve becomes:

$$Q_c - Q_R = 2Q_o(\nu - \delta\,\zeta_r)$$

Applying D'Alembert's rule-introducing viscous f effect and using equations (17), (22) and (2 following equation is obtained:

$$M_R . S_{lmax}\ddot{\zeta}_r + \beta S_{lmax}\dot{\zeta}_r = 2Q_o(\nu - \delta . \zeta_r)$$

or

$$t_{Mr}^2`. \ddot{\zeta}_r + t'_{Dr}. \dot{\zeta}_r + \delta . \zeta_r = \nu$$

where: the time constants t'_{Mr} and t'_{Dr} are:

$$t'_{Mr} = \sqrt{\frac{M_R \cdot S_{lmax}}{2Q_o}} \quad \text{and} \quad t'_{Dr} = \frac{\beta \cdot S_{lmax}}{2Q_o}$$

Dividing both sides of equation (26) by the proportionality δ we get:

$$t^2_{Mr} \cdot \ddot{\zeta}_r + t_{Dr} \cdot \dot{\zeta}_r + \zeta_r = \frac{\lambda}{l} v \qquad (27)$$

where:

$$\frac{\lambda}{l} = \frac{1}{\delta}, t^2_{Mr} = \frac{t'^2_{Mr}}{\delta} \text{ and } t_{Dr} = \frac{t'_{Dr}}{\delta}$$

Equation (27) describes the dynamics of the centrifugal governor. The well-known dynamic analysis of the hydraulic servomotor is shortly reproduced for convenience and completeness [15].

The servomotor, its steady state performance curves and the positions of the walking been during operation are demonstrated in Figure (5 a, b, c).

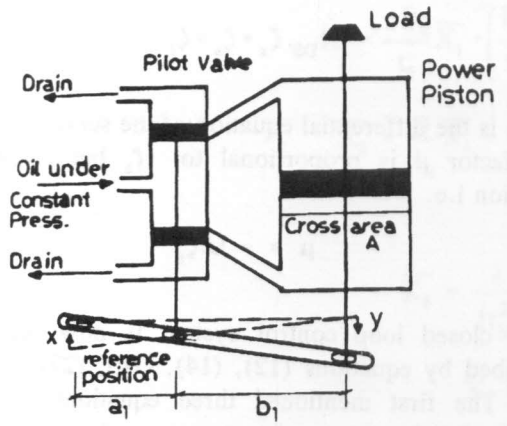

Figure 5-a. Four ways Hydraulic amplifier.

Let capital letters designate the parameters while small letters denote variations in these parameters. Friction and load effects are considered too.

Taylor expansion formula is adopted for linearization of non-linear relationships namely:

$$F(X,Y,Z) = F(X_o + \Delta X, Y_o + \Delta Y + Z_o + \Delta Z) +$$

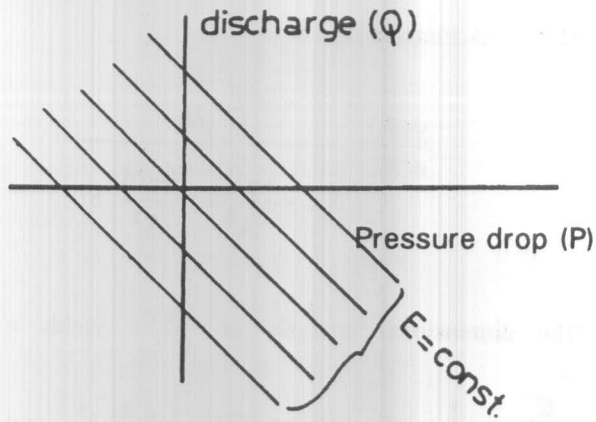

Figure 5-b. Sketch of the Steady state Performance (operating curves) of the Hydraulic amplifier.

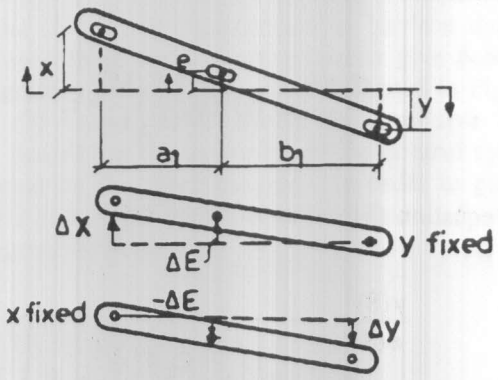

Figure 5-c. Analyzing the Displacements of the walking beam.

$$\sum_{J=1}^{j=\infty} \frac{1}{j!}\left(\frac{\partial F}{\partial X} \cdot \Delta X + \frac{\partial F}{\partial Y} \cdot \Delta Y + \frac{\partial F}{\partial Z} \cdot \Delta Z\right)^j$$

Neglecting second and higher order terms the following equations could be written:

$$\bar{q} = A\bar{y} = \frac{\partial Q}{\partial E}\Big|_{P=c} \cdot e + \frac{\partial Q}{\partial P}\Big|_{E=c} \cdot p' = c'_1 e - c'_2 \cdot p' \qquad (28)$$

But

$$p' = \frac{M}{A}\ddot{y} + \frac{\beta'}{A}\dot{y} \qquad (29)$$

Substituting equation (29) into equation (28) yields:

$$C'_1 e - C'_2 \frac{M}{A}\ddot{y} - C'_2 \frac{\beta'}{A}\dot{y} = A\dot{y} \qquad (30)$$

Hence the transfer function:

$$\frac{y(S)}{e(S)} = \frac{C'_1/A}{S\left[1 + \frac{C_2\beta'}{A^2} + \frac{C_2 M}{A^2}.S\right]} \quad (31)$$

The dimensional analysis of C'_1 yields s^{-1} and

$\frac{C'_1}{A} = \frac{1}{\tau'}$, the units of C_2 is $\frac{m^4.s}{kg_m}$ and that of

β' is $kg_f.s/m$ or kg_m/s. Then the units of $\beta' C_2 / A^2$ is dimensionless while the units of.

$$\frac{C_2 M}{A^2} \text{ is (s) i.e. } \frac{C_2 M}{A^2} = \tau_1$$

and equation (31) is transformed into:

$$\frac{y(S)}{e(S} = \frac{1}{\tau'.S\left\{\left(1 + \frac{C_2\beta'}{A^2}\right) + \tau_1.S\right\}} \quad (32)$$

Equation (32) describes the dynamics of an (I_1) control property servomotor. In engineering applications both τ_1 and $C_2 \beta'/A^2$ are almost negligible and equation (32) reduces to the known formula namely.

$$\frac{y(S)}{e(S)} = \frac{1}{\tau'.S} \quad (33)$$

which denotes an (I_0) control property servomotor. Attachment of the walking beam to this servomotor transforms its control property to (P_1). This is shortly displayed as follows:

$$e = \frac{\partial E}{\partial X}\Big|_{Y=c} x + \frac{\partial E}{\partial Y}\Big|_{X=c} y$$

$$= \lim_{\substack{\Delta E \to 0 \\ \Delta X \to 0}} \frac{\Delta E}{\Delta X}.x + \lim_{\substack{\Delta E \to 0 \\ \Delta Y \to 0}} \frac{\Delta E}{\Delta Y}.y$$

or

$$e = \frac{b_1}{a_1 + b_1}.x - \frac{a_1}{a_1 + b_1}.y \quad (34)$$

Substituting equation (34) into equation (33) gives:

$$\frac{y(S)}{x(S)} = \frac{b_1/(a_1 + b_1)}{\tau.S + a_1/(a_1 + b_1)} \quad (35)$$

In general $a_1 = b_1$ and equation (35) becomes:

$$\frac{y(S)}{x(S)} = \frac{1}{2\tau'.S + 1}$$

or

$$\frac{\zeta_s(S)}{\zeta_r(S)} = \frac{1}{t_{DS}.S + 1} \quad (36)$$

Where $\zeta_r(S) = x(S)$ = deviation in sleeve's displacement while $\zeta_s(S) = y(S)$ = deviation in servomotor's displacement and $t_{DS} = 2\tau' =$ the time delay of the servomotor. In time domain equation (36) is transformed to:

$$t_{DS}.\dot{\zeta}_s + \zeta_s = \zeta_r \quad (37)$$

which is the differential equation of the servomotor. The fuel factor μ is proportional to ζ_s but opposite in direction i.e.

$$\mu = -U.\zeta_s \quad (38)$$

The closed loop control system is now completely described by equations (12), (14), (16), (27), (37) and (38). The first mentioned three equations should be linearized to have a consistent system of equations.

The aforementioned Taylor's series are also used in linearizing these equations near the operating point. The following non-dimensional relative deviations or dimensionless constants are introduced in order to simplify the description of the dynamic behavior of the linearized control system after hard tedious manipulations:

$$\nu = \frac{n - n_o}{n_o}, \tau = \frac{T_4 - T_{40}}{T_{40}}, \psi = \frac{P_2 - P_{20}}{P_{20}}$$

$$p_d = \frac{N - N_o}{\dot{m}_o C_p T_1}, \quad \psi_{eo} = 1 - \left(\frac{P_5}{P_{40}}\right)^{\frac{\gamma-1}{\gamma}}, \quad \psi_{co} = \left(\frac{P_{20}}{P_1}\right)^{\frac{\gamma-1}{\gamma}} - 1$$

$$t_\theta = \frac{I\overline{\omega_o^2}}{\dot{m}_o c_p T_1}$$

$$\theta = \frac{T_{40}}{T_1}, \quad \alpha = \frac{C_{PT}}{C_{pc}}, \quad A_1 = 1 - \frac{T_{30}}{T_{40}},$$

and the system of equations reduces to:

$$B_2 = \frac{a\psi_{co}}{\eta_c}, C_1 = 0.5 + \frac{T_{30}}{T_{40}}, \quad C_2 = \tfrac{1}{2}\eta_t \theta \psi_{eo},$$

$$D_1 = 1 - \frac{T_{30}}{T_{40}} - \frac{P_{20}}{P_{40}}\left(\frac{dT_3}{dP_2}\right)_{at P_2 = P_{20}},$$

$$D_2 = \eta_t.\theta.\psi_{eo}\left[1 + \frac{(\gamma-1)}{\gamma}(1-\psi_{eo})\right] - \frac{\psi_{co}}{\eta_c}\left[b + \frac{\gamma-1}{\gamma}(1+\psi_{co})\right],$$

$$t_m = \frac{P_{20}}{\dot{m}_o} F(P_{20}) = \frac{P_{20}}{\dot{m}_o}\left(\frac{dm}{dP_2}\right)_{at\ "o"} \quad \text{and}$$

$$\left.\begin{aligned} B_2.\nu + C_2.\tau + D_2.\psi - P_d &= t_\theta.\dot{\nu} \\ a.\nu + \tfrac{1}{2}\tau + (b-1).\psi &= t_m.\dot{\psi} \\ C_1.\tau + D_1.\psi &= -A_1.U.\zeta_s \\ t_{DS}.\dot{\zeta}_s + \zeta_s &= \zeta_r \\ t_{Mr}^2.\ddot{\zeta}_r + t_{Dr}.\dot{\zeta}_r + \zeta_r &= \frac{\lambda}{l}\nu \end{aligned}\right\} \quad (39)$$

Equations (39) when transformed to Laplace domain and displayed in pictorial representations give both the block diagram and signal flow graph indicated in Figures (6) and (7) respectively. Moreover, the five state variables describing the dynamics of the control system are indicated on the block diagram. In order to get the state matrix and output matrix equations directly from the block diagram we write:

$$\left.\begin{aligned} \dot{\overline{X}}_1 &= \frac{-B_2}{t_\theta}\overline{X}_1 + \left(\frac{D_2}{t_\theta} - \frac{C_2 D_1}{t_\theta.C_1}\right)\overline{X}_2 - \frac{C_2 A_1 U}{t_\theta C_1}\overline{x}_5 - \frac{1}{t_\theta}P_d \\ \dot{\overline{X}}_2 &= \frac{a}{t_m}\overline{X}_1 + \frac{1}{t_m}\left[b - 1 - \frac{D_1}{2C_1}\right]\overline{X}_2 - \frac{A_1 U}{2C_1 t_m}\overline{X}_5 \\ \dot{\overline{X}}_3 &= \overline{X}_4 \\ \dot{\overline{X}}_4 &= \frac{\lambda}{l t_{Mr}^2}\overline{X}_1 - \frac{1}{t_{Mr}^2}\overline{X}_3 - \frac{t_{Dr}}{t_{Mr}^2}\overline{X}_4 \\ \dot{\overline{X}}_s &= \frac{1}{t_{DS}}\overline{X}_3 - \frac{1}{t_{DS}}\overline{X}_5 \end{aligned}\right\} \quad (40)$$

$$\begin{bmatrix} \dot{\overline{X}}_1 \\ \dot{\overline{X}}_2 \\ \dot{\overline{X}}_3 \\ \dot{\overline{X}}_4 \\ \dot{\overline{X}}_5 \end{bmatrix} = \begin{bmatrix} -B_2/t_\theta & (C_1D_2 - C_2D_1)/C_1 t_\theta & 0 & 0 & -C_2A_1.U/C_1 t_\theta \\ a/t_m & (2bC_1 - 2C_1 - D_1)/(2C_1 t_m) & 0 & 0 & -A1.U/2C_1 t_m) \\ 0 & 0 & 0 & 1 & 0 \\ \lambda/l t_{Mr}^2 & 0 & -1/t_{Mr}^2 & -t_{Dr}/t_{Mr}^2 & 0 \\ 0 & 0 & 1/t_{Ds} & 0 & -1/t_{Ds} \end{bmatrix}$$

$$\begin{bmatrix}\dot{\bar{X}}_1\\ \dot{\bar{X}}_2\\ \dot{\bar{X}}_3\\ \dot{\bar{X}}_4\\ \dot{\bar{X}}_5\end{bmatrix} = \begin{bmatrix}\bar{X}_1\\ \bar{X}_2\\ \bar{X}_3\\ \bar{X}_4\\ \bar{X}_5\end{bmatrix} + \begin{bmatrix}-1/t_\theta\\ 0\\ 0\\ 0\\ 0\end{bmatrix} P_d \quad \text{and} \quad \nu = [1\ 0\ 0\ 0\ 0] \begin{bmatrix}\bar{X}_1\\ \bar{X}_2\\ \bar{X}_3\\ \bar{X}_4\\ \bar{X}_5\end{bmatrix}$$

or $[\ \dot{\bar{X}}\ ] = [\ \bar{P}\ ][\ \bar{X}\ ] + [B]\, P_d$ and $C = [L][\ \bar{X}\ ]$, where:

$$\begin{bmatrix}\overline{X_1}\\ \overline{X_2}\\ \overline{X_3}\\ \overline{X_4}\\ \overline{X_5}\end{bmatrix} = \begin{bmatrix}\nu\\ \psi\\ \zeta_r\\ \dot{\zeta}_r\\ \zeta_e\end{bmatrix}$$

and

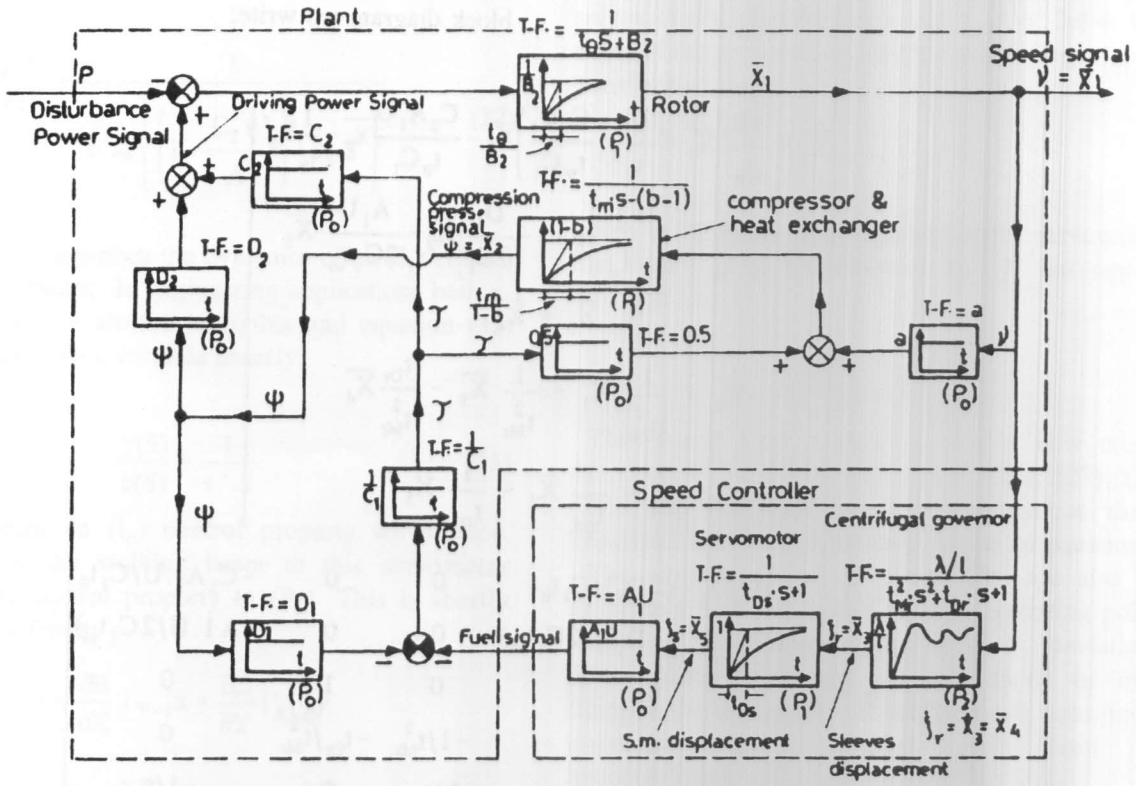

Figure 6. Block Diagram of the control system Illustrating Transfer functions, control properties, unit step responses and state variables.

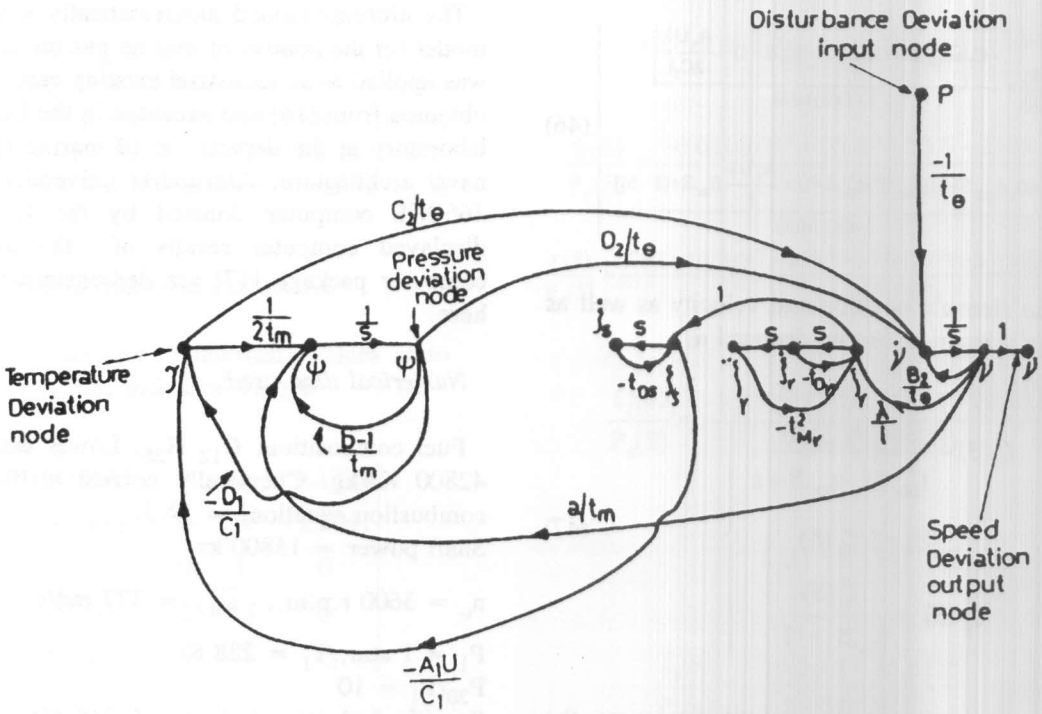

Figure 7. Signal flow graph of the control system.

$$\tau = -\frac{1}{C_1}\,(D_1\psi + A_1.U.\zeta_s) \qquad (42)$$

It is to be noted that all state variables here are physical, measurable values. From basic control theories the solution of equation (42) is:

$$\left.\begin{aligned} [\bar{X}(t)] &= L^{-1}[S[\bar{I}] - [\bar{P}]]^{-1}.[\bar{X}(o)] + \int_{\bar{\epsilon}=o}^{\bar{\epsilon}=t} [\phi(t-\bar{\epsilon})][B]P_d(\bar{\epsilon})\,d\,\bar{\epsilon} \\ \text{and} \quad C(t) &= [L[\bar{X}(t)] \\ \text{where} \quad [\phi(t)] &= L^{-1}[S[\bar{I}] - [\bar{P}]]^{-1} = e^{[\bar{P}]t} \\ \text{The characteristic equation is:} \quad 1 + G(S)H(s) &= \det[S[\bar{I}] - [\bar{P}]] = 0 \end{aligned}\right\} \qquad (43)$$

or

$$1 + G(S)H(S) = \frac{A_1 U\lambda}{1}[C_2(t_m.S + 1 - b) + \frac{D_2}{2}] +$$

$$a(C_2D_1 - C_1D_2)(t_{DS}.S+1)(t_{Mr}^2.S^2 + t_{Dr}.S+1) +$$

$$C_1(t_\theta.S+B_2)(t_{De}.S+1)(t_{Mr}^2.S^2 + t_{Dr}.S+1)(t_m.s + 1 - b + \frac{D_1}{2C_1}) \qquad (44)$$

The closed loop transfer function $\nu(s)/P_d(s)$ could be determined either from the block diagram reduction algebra or from equations (43).

$$\frac{\nu(s)}{P_d(s)} = \frac{-C_1(t_{DS}.S+1)(t_{Mr}^2.S^2 + t_{Dr}.S+1)(t_m.s + 1 - b - \frac{D_1}{2C_1})}{1 + G(S)H(S)}$$

$$= \frac{[L]\,\mathrm{adj}\,[S[\bar{I}] - [\bar{P}]]\,[B]}{\det[S[\bar{I}] - [\bar{P}]]} \qquad (45)$$

The other dynamic parameters in the system particularly pressure and temperature deviations (ψ and τ) could be similarly deduced from the block diagram or from equations (42) and (43); these transfer functions are:

$$\left.\begin{aligned}\frac{\psi(S)}{P_d(S)} &= \frac{-C_1\left[a(t_{DS}.S+1)(t_{Mr}^2.S^2+t_{Dr}.S+1)-\frac{A_1 U\lambda}{2C_1 l}\right]}{1+G(S)H(S)}\\ \text{and}\\ \frac{\tau(S)}{P_d(S)} &= \frac{aD_1(t_{Ds}.S+1)(t_{Mr}^2.S^2+t_{Dr}.S+1)+\frac{A_1 U\lambda}{l}[t_m.S+(1-b)]}{1+G(S)H(S)}\end{aligned}\right\} \quad (46)$$

Similarly, the sleeve's position and velocity as well as the servomotor's Position can be deduced as:

$$\left.\begin{aligned}\zeta_r(S) &= \frac{\nu(S).)\lambda/l)}{t_{Mr}^2.S^2+t_{Dr}.S+1}\\ \dot{\zeta}_r(S) &= S.\zeta_r(S)\\ \zeta_s(S) &= \frac{\zeta_r(S)}{t_{Ds}.S+1}\end{aligned}\right\} \quad (47)$$

In order to evaluate the relative stability measures, the open loop transfer function G(S).H(S) should be calculated either from the block diagram or by subtracting one from [1+G(S) H(S)]. The manipulation results in:

$$G(S)H(S) = \frac{\text{numerator}}{\text{denominator}}$$

where:

$$\text{numerator} = 2aC_2D_1t_{Ds}t_{Mr}^2S^3 + 2aC_2D_1(t_{Ds}.t_{Dr}+t_{Mr}^2).S^2 + \left[2aC_2D_1(t_{DS}+t_{Dr}) + \frac{2C_2.A_1.\lambda.t_m}{l}\right].S + \left[\frac{2C_2A_1U\lambda(1-b)}{l} + 2aC_2D_1\right]$$

and

$$\text{denominator} = 2C_1.t_m.t_\theta t_{DS}.t_{Mr}^2\left(S+\frac{B_2}{t_\theta}\right)\left(S+\frac{1}{t_{DS}}\right)* *\left(S+\frac{2C_1(1-b)+D_1}{2C_1.t_m}\right)\left(S^2+\frac{t_{Dr}}{t_{Mr}^2}.S+\frac{1}{t_{Mr}^2}\right) \quad (48)$$

Illustrative Case Study:

The aforementioned mathematically analyzed dynamic model for the control of marine gas turbine power plants was applied to an industrial existing case whose data was obtained from [16] and executed in the Lloyd's computer laboratory at the department of marine engineering and naval architecture, Alexandria university on the DELL 466/ME computer donated by the L.R. Graphically displayed computer results of the used MATLAB computer package [17] are demonstrated and discussed here.

Numerical data used:

Fuel composition: $C_{12}H_{26}$. Lower calorific value = 42800 KJ/kg. Chemically correct air/fuel ratio (from combustion equation) = 14.3
Shaft power = 15800 kw

n_o = 3600 r.p.m., $\bar{\omega}_o$ = 377 rad/s

P_1 = 1 atm, T_1 = 288 K
P_{20}/P_1 = 10
Specific fuel consumption = 0.316 kW.hr
Fuel consumed = 1.384 kg/s, air flow = 78.2 kg/s, excess air factor = 3.95
η_c = 0.88, η_t = 0.78, γ_{air} = 1.4

$$T_{20} = \left(\frac{P_{20}}{P_1}\right)^{\gamma-1}.T_1 = 732\ \text{K},$$

$$T'_{20} = T_1 + \frac{T_2 - T_1}{\eta_c} = 792\ \text{K}$$

T_{40}=-1211 K, T'_{50}=755 K, C_{pc}=1.005 KJ/Kg.K, C_{PT}=1.1305 KJ/Kg.K
α=1, Torque=42.64 KN.m, mass moment of inertia=101.8 Kg. m^2. Hence: ψ_{co}=0.482, ψ_{co}=0.9306, Θ=4.2.

Either from heat released rate, gas flow rate, gas temperature rise and CP_T or from thermal balance of heat exchanger T_{30} and hence A_1 could be calculated.

A_1=0.537, B_2=1.4805, C_2=0.7895, D_2=1.441, C_1=0.9628, D_1=0.35, t_Θ=18 s, U=5, $t_{Dr}=t_{DS}$=0.2 s, t^2_{Mr}=0.04 s^2, λ/l=20, a=1.4, b=-0.2.

To simplify determining t_m instead of manipulating cumbersome analytical functions, some assumptions are made:
Density of compressed air = P/RT = 4.223 kg/m^3, its specific volume = 0.2368 m^3/kg.

Air volumetric flow = 78.2 * 0.2368 = 18.518 m^3/s

A heat exchanger having about 2.5 m diameter and a similar value in length with 0.02 m inner tube diameter and pitch diameter ratio reaching about 3 yields $t_m = 1$ s.

In order not to violate the validity of the linearized control model, the external disturbance deviation P_d is taken as 10%.

Numerically Substituted Mathematical Model:

Substituting the preceding numerical values into equations from (41) to (48) inclusive we get:

$$[\bar{P}] = \begin{bmatrix} -0.0822 & 0.0641 & 0 & 0 & -0.1223 \\ 1.4 & -0.9817 & 0 & 0 & -1.3941 \\ 0 & 0 & 0 & 1 & 0 \\ 500 & 0 & -25 & -5 & 0 \\ 0 & 0 & 5 & 0 & -5 \end{bmatrix}$$

$$[B] = \begin{bmatrix} -0.0556 \\ 0 \\ 0 \\ 0 \\ 0 \end{bmatrix}, \quad [L] = [1 \ 0 \ 0 \ 0 \ 0]$$

$$P_d = 0.1 \ , \ P_d(S) = \frac{0.1}{S}$$

$$\det [S[\bar{I}] - [\bar{P}]] = 1 + G(S)H(S) =$$

$$= 0.1387(S^5 + 11.4614S^4 + 64.6496S^3 + 198.3944S^2 + 489.8176S + 648.739)$$

whose roots are:

$$-4.187 \pm j3.2765, \ -0.283 \pm j3.0037 \text{ and } -2.5215$$

The values of roots insure the absolute stability, however predict that the system is severely oscillatory.

$$\frac{v(s)}{P_d(s)} = \frac{-7.704 * 10^{-3}(S^4 + 11.3875S^3 + 63.8125S^2 + 194.0875S + 172.7125)}{1 + G(S)H(S)}$$

whose zeros are:

$$-2.4984 \pm j4.3264, \ -5.0094 \text{ and } -1.3813$$

$$\frac{\psi(S)}{P_d(S)} = \frac{-0.0108(S^3 + 10S^2 + 50S - 2364.4286)}{1 + G(S)H(S)}$$

$$\frac{\tau(S)}{P_d(S)} = \frac{3.92 * 10^{-3}(S^3 + 10S^2 + 13748.9796S + 16563.4439)}{1 + G(S)H(S)}$$

$$\frac{\zeta_r(S)}{P_d(S)} = \frac{-3.852S^2 - 24.5815S - 26.6115}{1 + G(S)H(S)}$$

$$\dot{\zeta}_r(s) = S.\zeta(S)$$

$$\frac{\zeta_s(s)}{P_d(s)} = \frac{-19.26S - 26.6115}{1 + G(s)H(S)} \quad \text{and}$$

$$G(S)\ H(S) =$$

$$= \frac{-0.01245S^3 - 0.1245S^2 + 41.7744S + 88.0109}{0.13875S^5 + 1.5905S^4 + 8.9788S^3 + 27.6421S^2 + 26.1633S + 1.9693}$$

whose zeros are:

$$-62.1545, \ -2.0965 \text{ and } +54.251 \text{ and}$$

whose poles are:

$$-2.4979 \pm J\,4.327, \ -5.0078, \ -1.3813 \text{ and } -0.0822$$

It is evident that all poles of the open loop transfer function G(S).H(S) lie in the left hand side of the complex plane.

The above mentioned relationships are analyzed in both frequency and time domains by the MATLAB package.

RESULTS AND DISCUSSION

The polar plot of the open loop transfer function G(S). H(S) when $S = j\omega$ is represented in Figure (8-a), whereas only the high frequency portion of this polar plot is indicated in Figure (8-b).

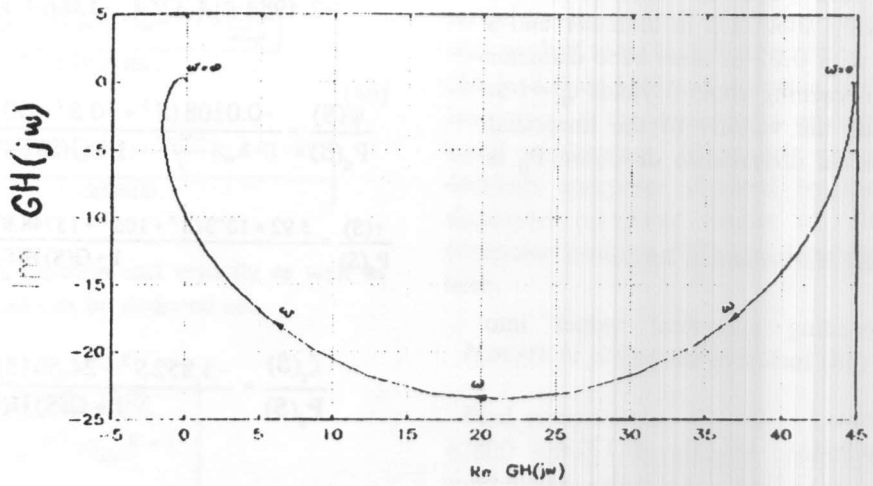

Figure 8-a. Polar plot.

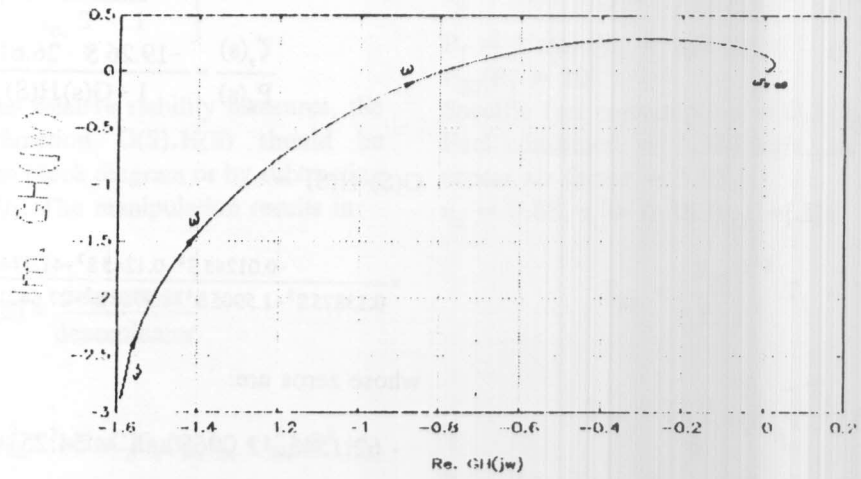

Figure 8-b. High frequency portion of polar plot.

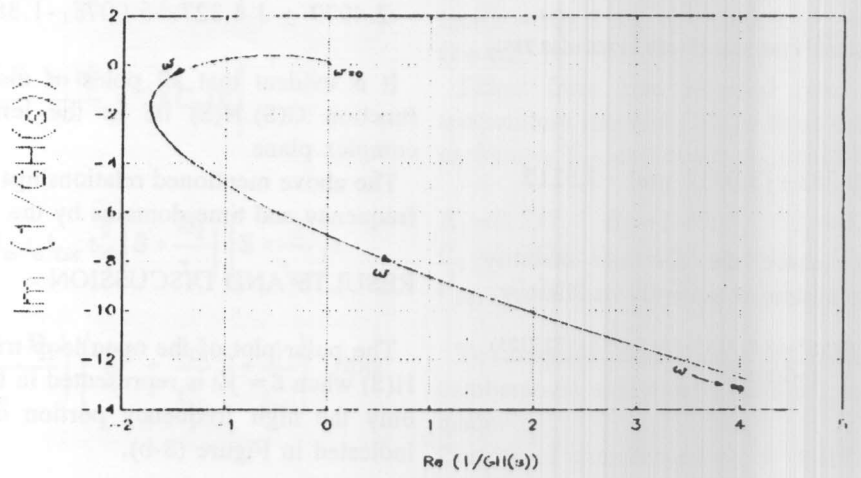

Figure 9. Inverse polar plot.

The aim being to study both the absolute and relative stability of the control system under discussion.

Figure (9) displays the inverse polar plot namely, $1/G(J\omega)\ H(J\omega)$ with the objective to enlarge and clarify the end portion of the polar plot $G(j\omega)\ H(J\omega)$ of higher values of the frequency ω which are extremely crowded in a minute portion in Figure 8 (a,b).

Concerning the absolute stability two graphical criteria are investigated. The Nyquist stability criterion plot is the result of the conformal mapping of the Nyquist path Figure (10-a) namely $S = \pm j\omega$ and $S = \lim_{r \to \infty} re^{J\phi}$, $90° \leq \phi \leq -90°$ on the open loop transfer function G(S)H(S). The conformally mapped Nyquist path is illustrated in the Nyquist stability plot shown in Figure (10-b). It is evident that the number of encirclements of this plot around the point (-1,0) equals zero.

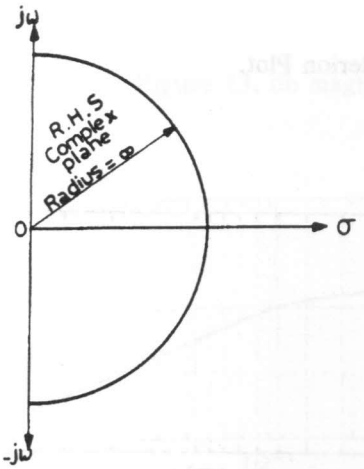

Figure 10-a. Nyquist path.

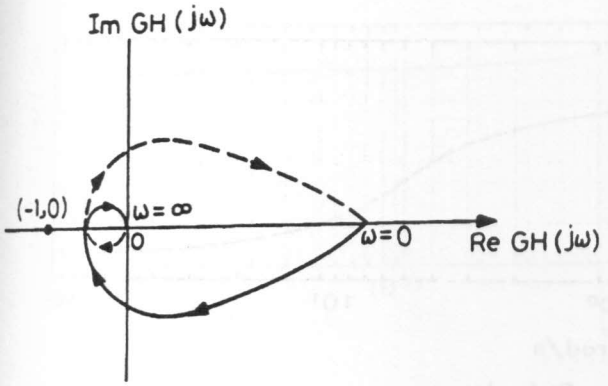

Figure 10-b. Sketch (not to scale) of the Nyquist stability criterion plot.

Since the number of the poles of the open loop transfer function located in the right hand side of the complex plane is also zero, the closed loop control system is absolutely stable.

The other pictorial graph for the absolute stability is the Mikhailov's plot of $1 + G(j\omega)\ H(j\omega)$ shown in Figure (11). All the absolute stability conditions are satisfied since the plot starts at the real axis at $\omega=0$, turns in an anticlockwise direction, intersects the quadrants in sequential order and the plot is terminated at $\omega = \infty$ in the fifth (first) quadrant corresponding to the highest power of S in the polynomial $1 + G(S)\ H(S)$. If the absolute stability is guaranteed for the control system, the question now is how far is the system from the border of instability or in other words, what is the relative stability whose measures are the gain and phase margins.

The gain and phase margins as investigated for the open loop transfer function from the enlarged high frequency portion of the polar plot Figure (8-b), from the Bode plots Figure (12) as well as from the decibel magnitude versus phase angle plot Figure (13) are as follows:

The phase crossover frequency $\omega_\pi = 3.2424$ rad/s

The gain crossover frequency $\omega_1 = 2.7050$ rad/s.

$$\text{The gain margin} = \frac{!}{|GH(j\omega_\pi)|} = 1.2614 \text{ (about 2 db)}$$

$$\text{The phase margin} = [180° + \arg GH(j\omega_1)] = 14.8158 \text{ degrees}$$

This reveals rather poor margins of stability which could be of course improved either by changing some design data or by compensation techniques (sate feedback concept in contemporary modern control theories).

Investigations of the characteristics of the automatic (closed loop) control system in the frequency domain are demonstrated in Bode Plots for the speed, pressure, temperature, sleeve's and servomotor's displacement deviations in Figures (14) through (18) respectively.

The resonant frequency ω_p occurs always at 2 rad/s with a resonant peak $M_p = \max |$ db magnitude ratio of the frequency function $|$ ranging from about -20 db to 15 db.

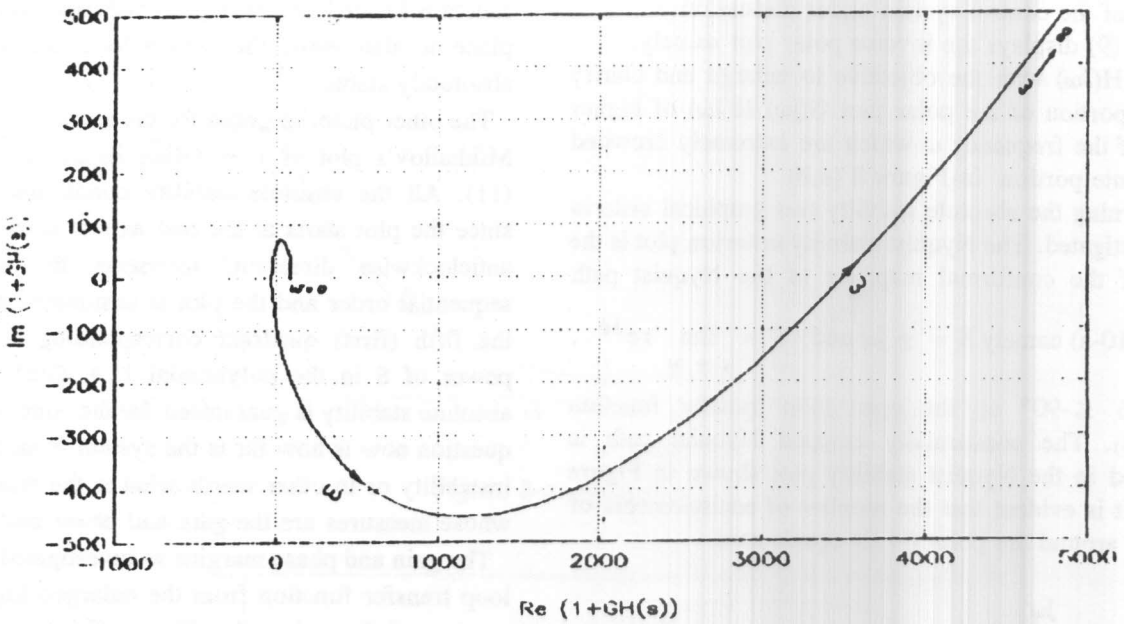

Figure 11. Mikhailov's Stability Criterion Plot.

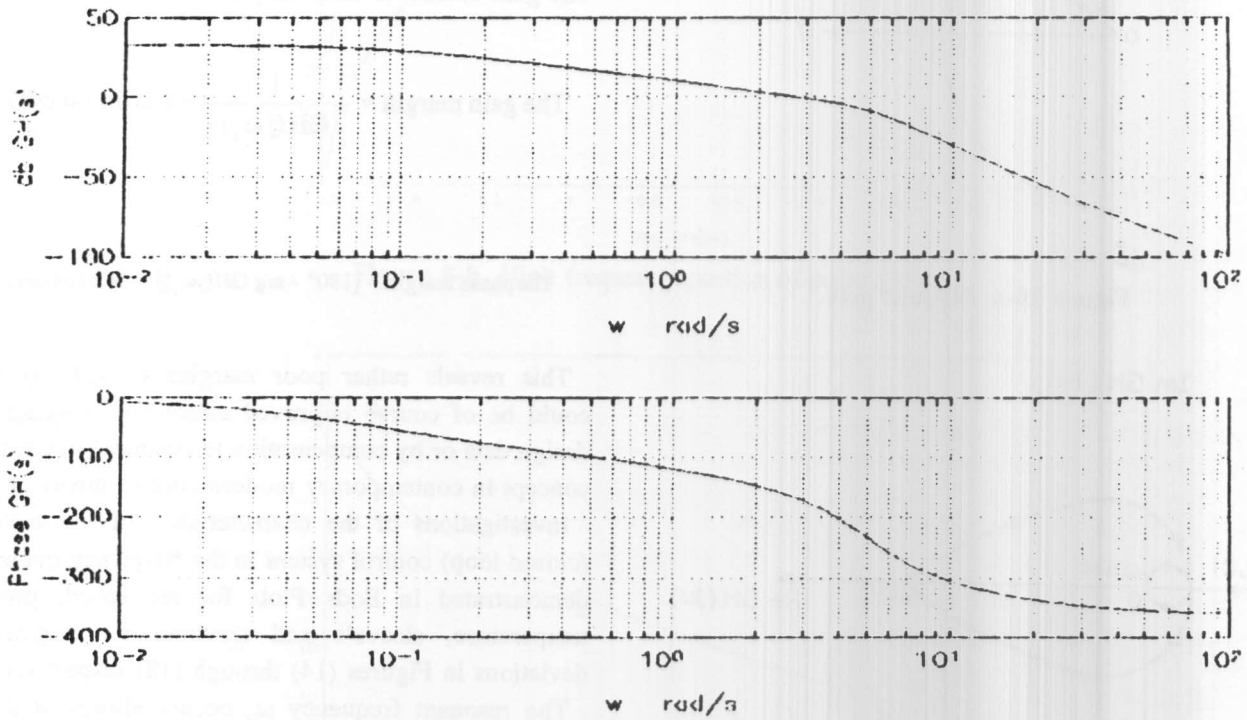

Figure 12. Open loop Bode plots.

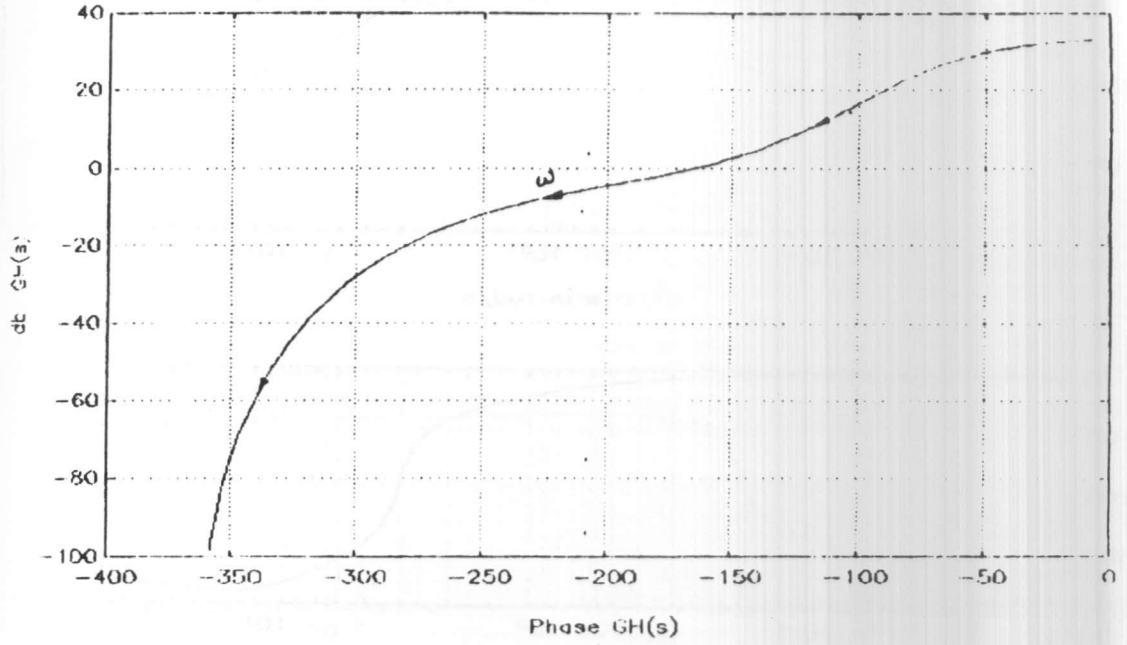

Figure 13. db magnitude versus phase angle plot of open loop.

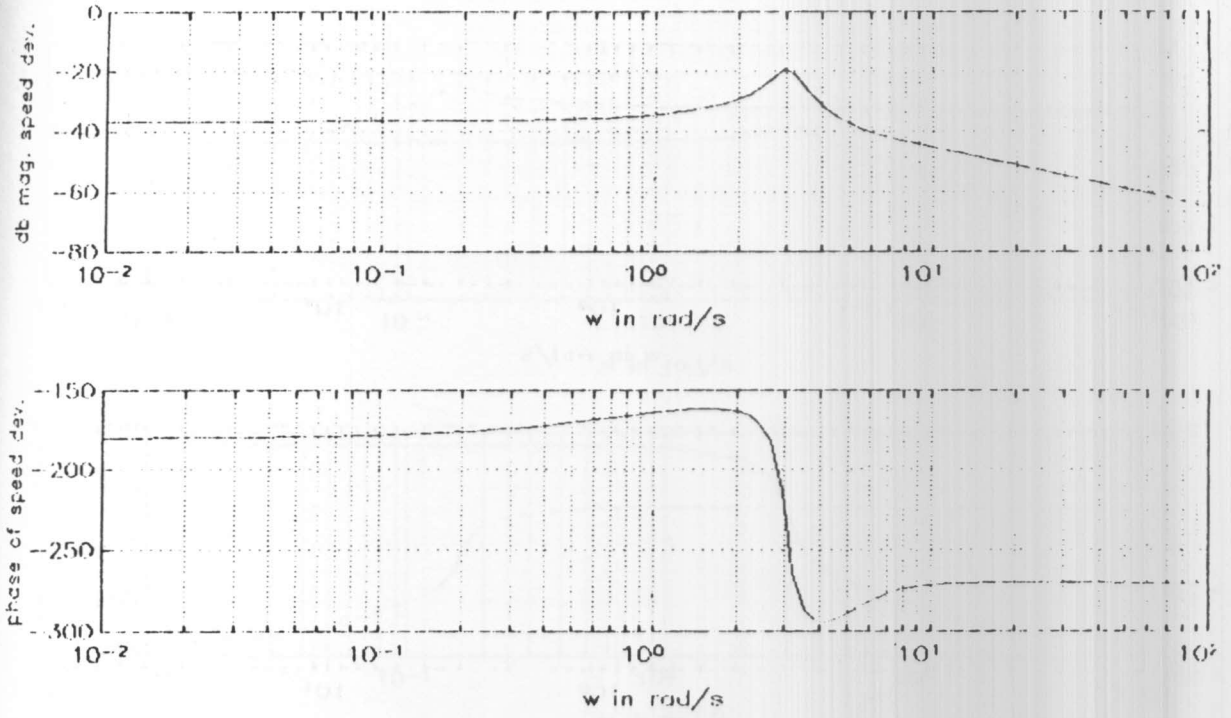

Figure 14. Bode plots of speed deviation (Closed loop).

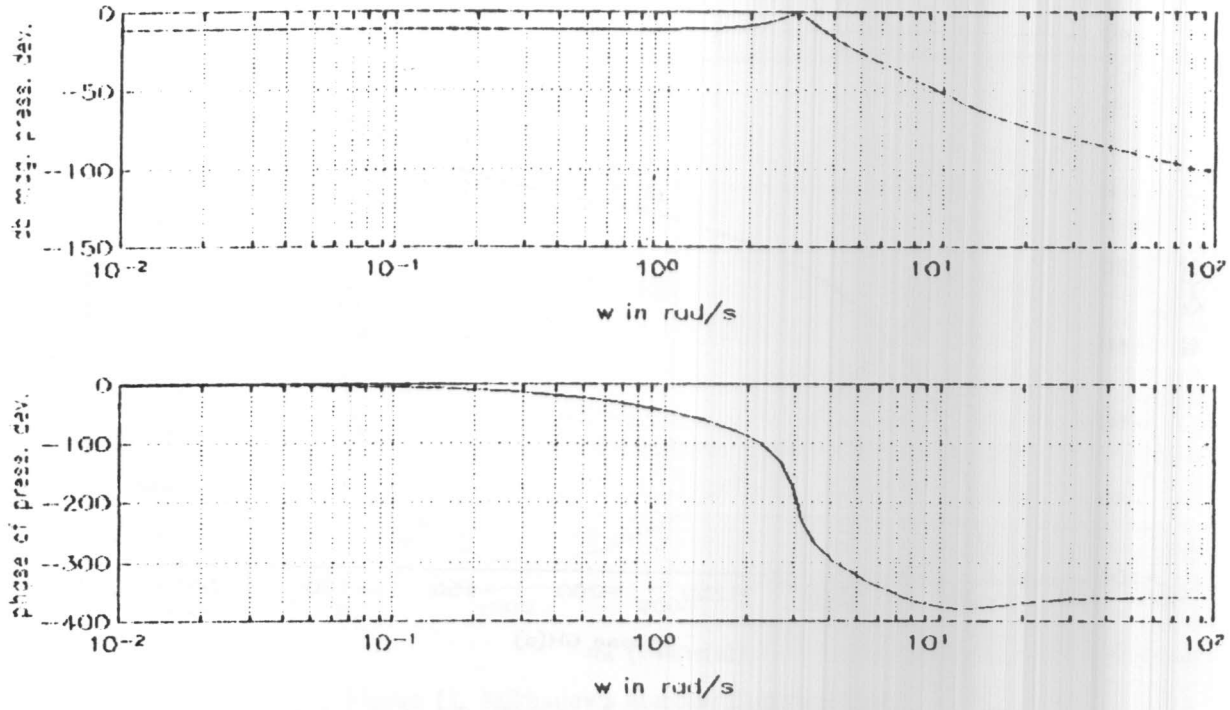

Figure 15. Bode plots of pressure deviation (Closed loop).

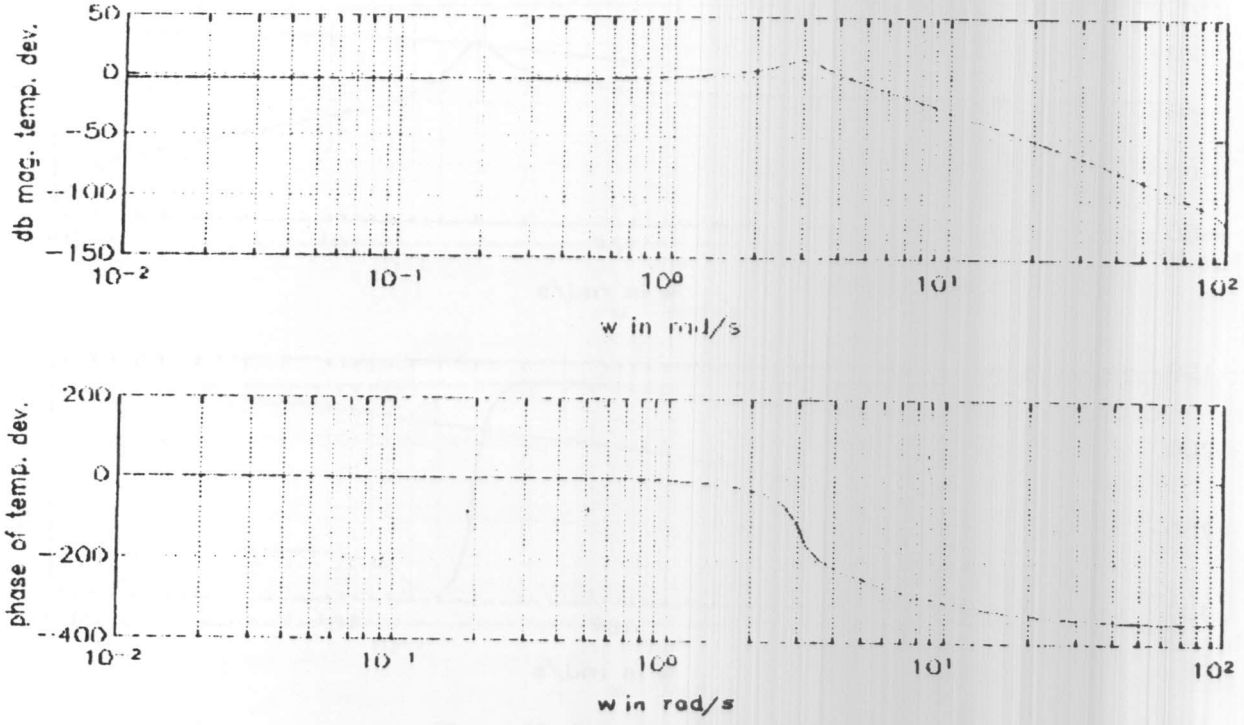

Figure 16. Bode plots of temperature deviation (Closed loop).

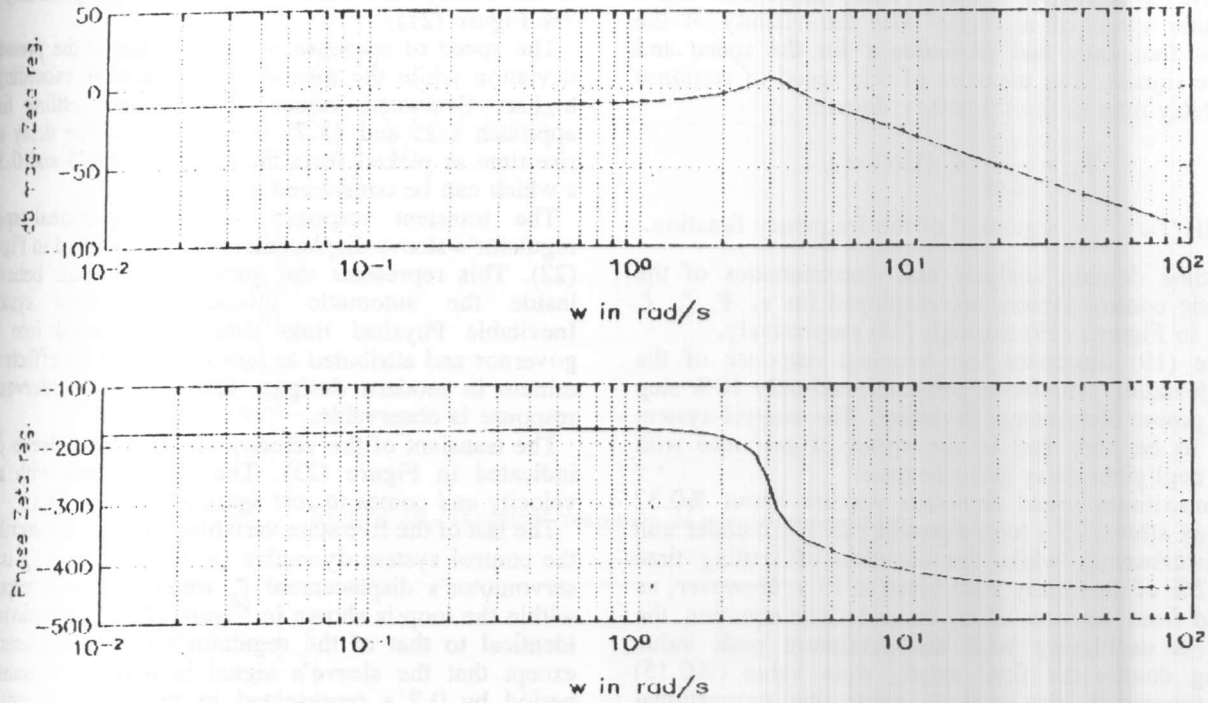

Figure 17. Bode plots of regulator's sleeve displacement.

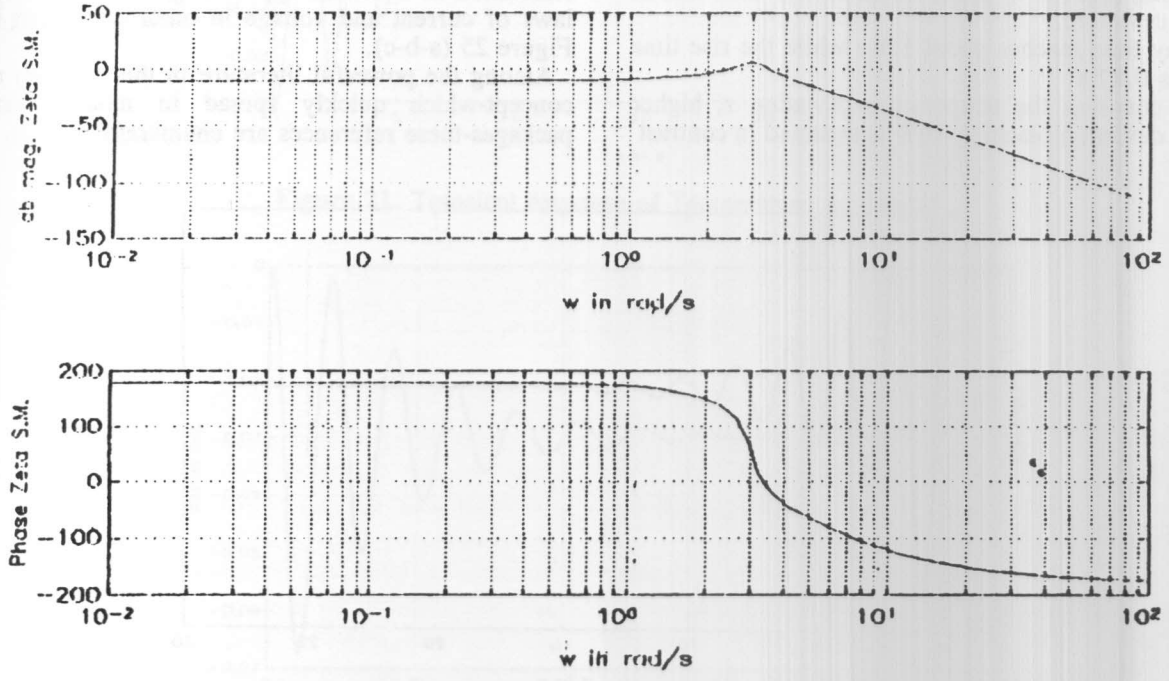

Figure 18. Bode plots of servomotor's displacement.

The system possesses a rather wide bandwidth with a reasonable speed of response near the vicinity of the resonant frequency and particularly for the speed and pressure signals. The measure of this speed of response is the delay time in the frequency domain

$$T_d = \frac{-d}{d\omega} \measuredangle GH(J\omega),$$

$\measuredangle GH(J\omega)$ = argument of the frequency function.

The time domain analysis and characteristics of the automatic control system are displayed for ν, Ψ, ζ_r, $\dot{\zeta}_r$ and ζ_s in Figures (19) through (25) respectively.

Figure (19) illustrates the transient response of the speed deviation ν under-as prementioned-only 10% step rise in power disturbance deviation. The control system proves to be very fast in the speed of response with almost negligible delay and rise time.

The maximum speed deviation reaches about %0.32 occurring after 0.75 s (corresponding to %3.2 under unit step disturbance), while the duration of settling time within 2% of the steady state value is 15 s. However, as revealed from the roots of the characteristic equation, the system is oscillatory with the maximum peak value reaching double the final steady state value (%0.15) which represents also a static error due proportional regulation of speed.

The maximum pressure deviation Figure (20) approaches 4% , whereas the steady state value is approximately %2.85. The Peak and settling time are about 1.5 and 10 s respectively. The speed of response, despite being high, is to some extent slower than that of the speed deviation.

The delay time reaches about 1.1 s while the rise time approaches 0.87 s.

In what concerns the temperature deviation τ, higher maximum deviation reaching 16% is assumed in contrast to the steady state value which lies in the proximity o 7% Figure (21).

The speed of response is close to that of the pressur deviation while the maximum overshoot is exceedingl higher. Evaluated values of peak and settling tim approach 1.25 and 13.75 s respectively. The delay an rise time as picked from the graph are 0.625 and 0.37 s which can be considered negligible.

The transient response of the proportional speed regulator's sleeve displacement ζ_r is displayed in Figur (22). This represents the governor's dynamic behavio inside the automatic closed-loop control system. Inevitable Physical time delay incorporated into the governor and attributed to inertia and friction effects are minute in modern designs, therefore swift intervening response is observable.

The transient of the velocity of regulator's sleeve $\dot{\zeta}_r$ is indicated in Figure (23). The sleeve starts with zero velocity and comes to rest again after about 15 s.

The last of the five state variables completely describing the control system dynamics (ν, ψ, ζ_r, $\dot{\zeta}_r$ and ζ_s) is the servomotor's displacement ζ_s whose transient response within the loop is shown in Figure (24). The behavior is identical to that of the regulator's sleeve displacement except that the sleeve's signal is delayed in transient period by 0.2 s represented in reducing the resulting intervention signal and this reduction vanishes in steady state.

At the termination of this discussion it may be convenient to introduce an up to date technique namely a dynamic model for the control system in Bond Graph simulation as a unified approach generalizing Kirchoff's laws of current and voltage in other engineering fields Figure 25 (a-b-c).

Among the powerful literature in this relatively recent concept-which quickly spread in modern computer packages-these references are enumerated [18-33].

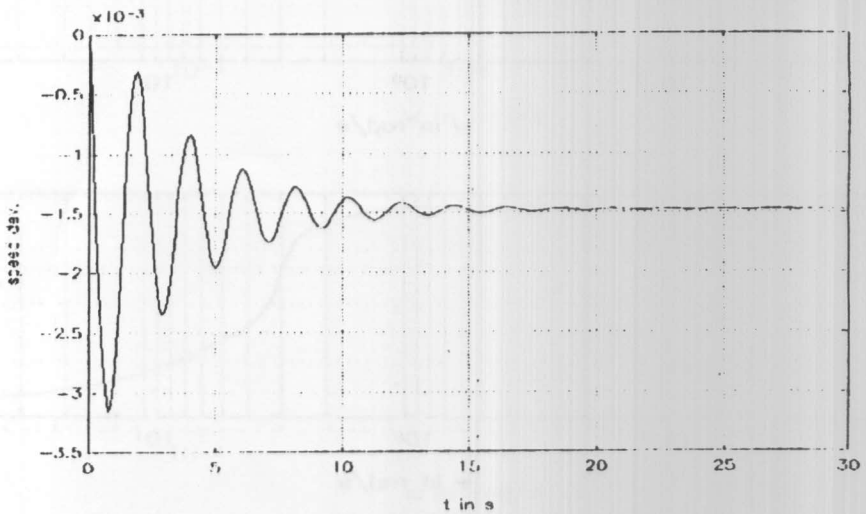

Figure 19. Transient response of speed deviation.

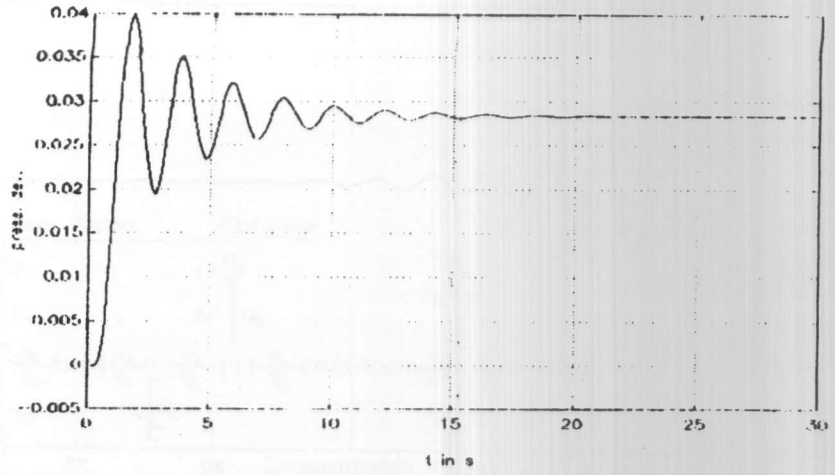

Figure 20. Transient response of pressure deviation.

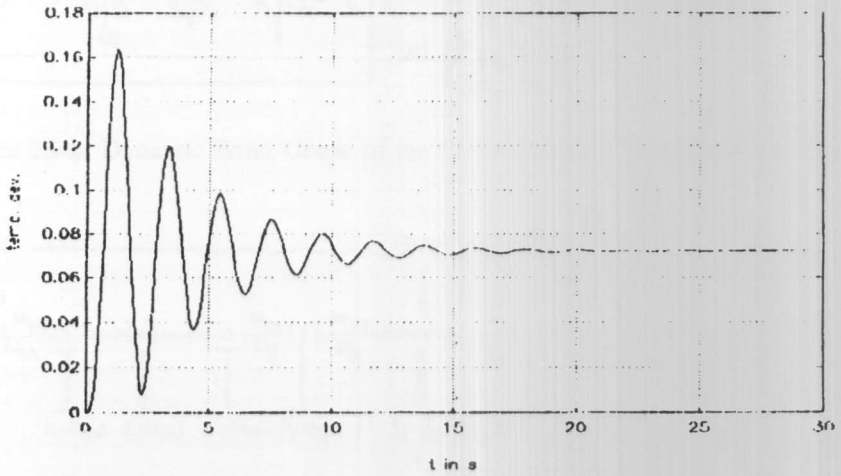

Figure 21. Transient response of Temperature deviation.

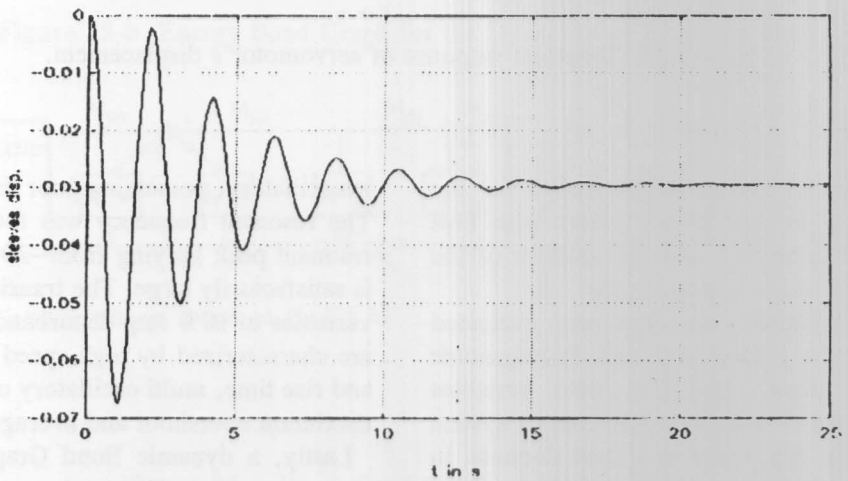

Figure 22. Transient response of regulator's sleeve displacement.

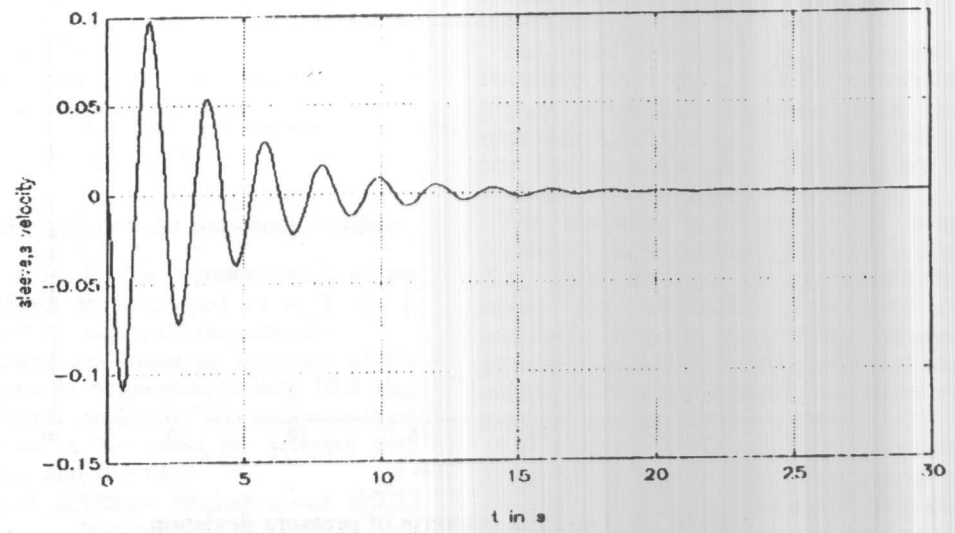

Figure 23. Transient response of regulator's sleeve velocity.

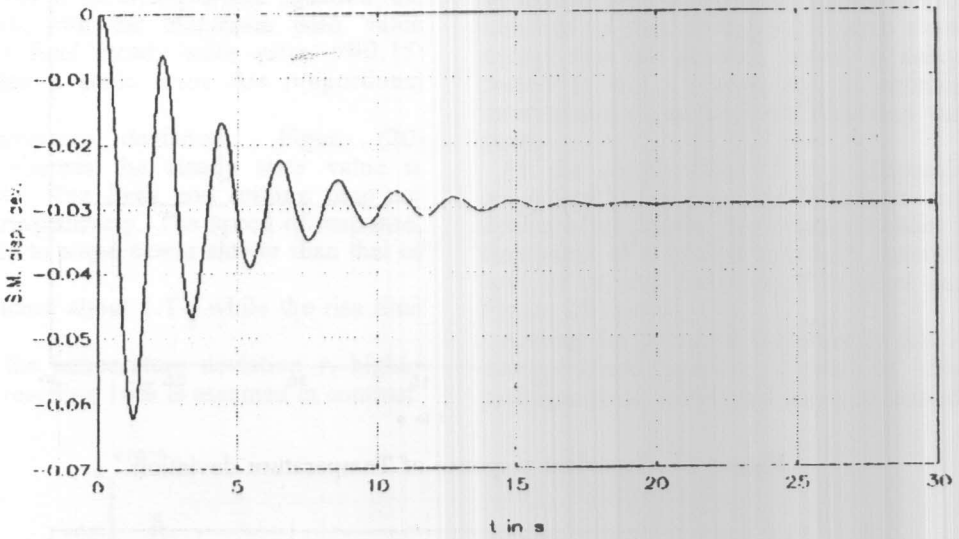

Figure 24. Transient response of servomotor's displacement.

CONCLUSION

The derived non-linear mathematical model for the control of marine gas turbine power plants with heat exchangers has been linearized and the validity of the model has been tested with a practical case.

Absolute and relative stability measures were evaluated in Nyquist, Mikhailov's, polar, Bode and db magnitude versus phase angle plots. The five state variables describing the dynamics of the automatic control system have been analyzed in frequency and time domains in search of their specifications. Characteristically, the selected system insures the absolute stability, however it is oscillatory, possessing poor relative stability measur The resonant frequency was found to be 2 rad/s wit resonant peak varying from -20 to 15 db; the bandwi is satisfactorily large. The transient responses of the st variables to 10% step disturbance power deviation sig are characterized by high speed of response, short de and rise time, multi oscillatory overshoots with excessi maximum overshoot and average settling time.

Lastly, a dynamic Bond Graph model of the cont system has been suggested.

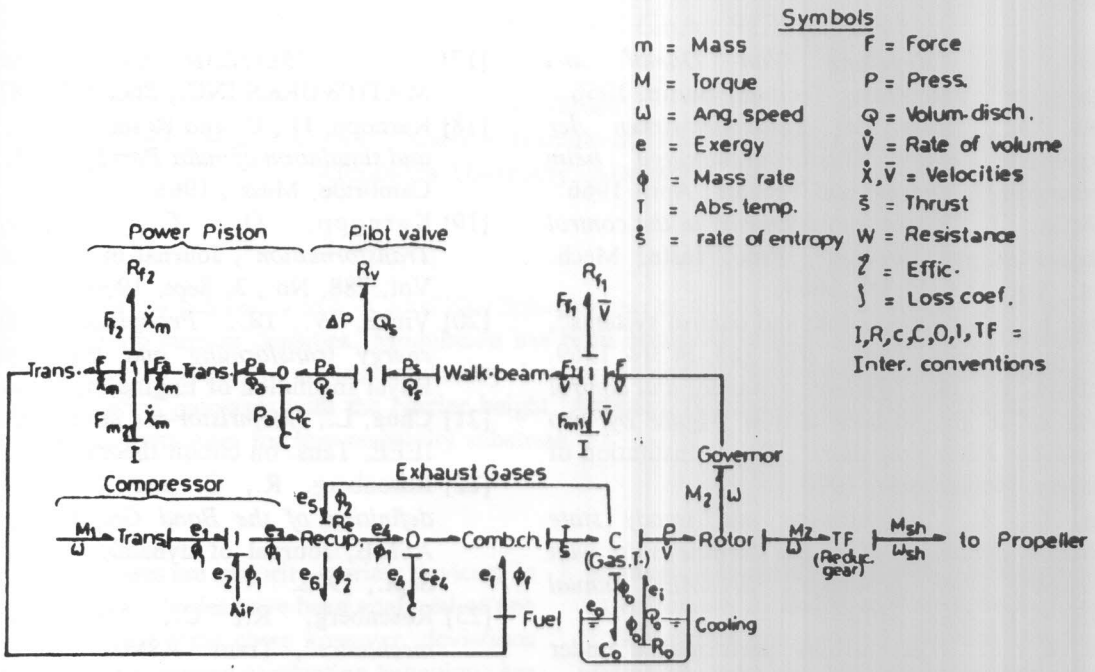

Figure 25-a. Dynamic Bond Graph of thr Controlled Gas Turbine Power Plant.

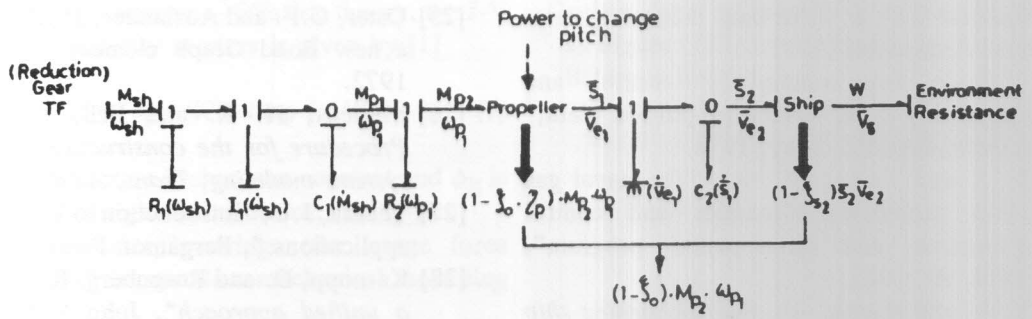

Figure 25-b. Energy Bond Graph for the Dynamics of Propeller Shaft.

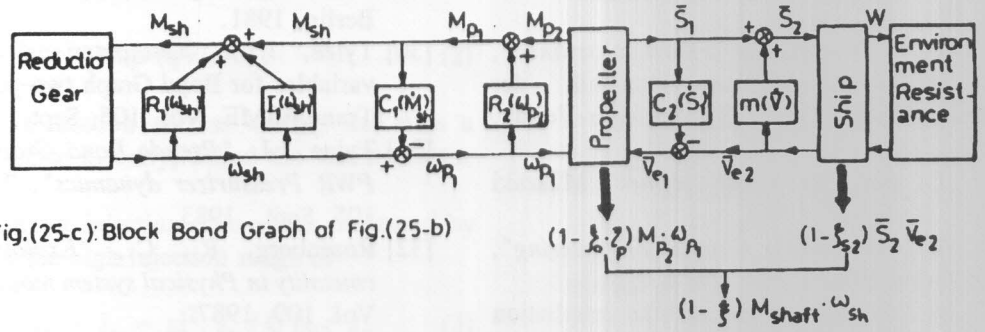

Fig.(25-c): Block Bond Graph of Fig.(25-b)

Figure 25-c. Block Bond Graph of Figure (25-b).

REFERENCES

[1] Kirilov, I., *"Regelung Von Dampf und Gasturbinen"*, Veb Verlag Technik, Berlin, 1956.

[2] Harms, A., *"über das zusammenwirken der Anlagenteile einer Gasturbinenanlage beim Regelvorgang"*, Energie und Technik, April 1966.

[3] Mc Arthur, J., *"Recent developments in the control of industrial gas turbines"*, Proc. Instn. Mech. Engrs., Vol. 183, Pt 3N, 1969.

[4] Warne, E., *"Gas* turbine fuel and control systems", PRoc. Instn. Mech. Engrs., Vol. 183, Pt 3N, 1969.

[5] Schatborn, W., IR., *"Systems dynamics and control aspects of a gas turbine driven frigate by two controllable Pitch propellers"*, Royal Institution of Engineers, Netherlands, 1970.

[6] Rubis, C., J., *"Acceleration and steady state propulsion dynamics of a gas turbine ship with controllable pitch propeller,, SNAME, Annual meeting N.Y., Nov., 1972.*

[7] Rubis, C., J., "Gas turbine performance under varying torque propeller loads", Int. Shipbuilding progress, Jan., 1974.

[8] Rubis, C., J. and Harper T., R., *"Reversing dynamics of a gas turbine ship with controllable pitch properller"*, Proc. fifth ship control systems symposium, Annapolis, 1978.

[9] _____, "Guide for centeralized control and automation of ship's gas turbine propulsion plant," *T & R Bulletin, SNAME,* May, 1978.

[10] Rubis, C., J. and Harper, T., R., "The naval gas turbine ship propulsion dynamics and control systems research and development program", SNAME Vol. 90, 1982.

[11] Rubis, C., J., and Harper, T., R., *"Governing ship propulsion gas turbine engines"*, SNAME, Vol. 94, PP-283-308, 1986.

[12] Száday, R., *"Gözturbinák"*, Tankönyv kiadó, Budapest, 1961.

[13] Traupel, W., *"Thermische Turbomaschinen"*, zweiter Band, 2 auf.,-zur Dynamik der Gasturbinenregelung-Seite 125, Springer-Verlag, Berlin 1968.

[14] Száday, R., *"A szabályozáselmélt elemei"*, Műszaki Könyvkiadó, Budapest, 1972.

[15] Raven, H., F., *"Automatic Control Engineering"*, 3rd ed., McGraw-Hill, Tokyo, 1978.

[16] _____, "LM 2500 Marine gas turbine installation design manual", General Electric marine and industrial Project department, U.S.A, July 1974.

[17] _____, *"MATLAB computer package"*, MATHWORKS INC., Stanford, 1987.

[18] Karnopp, D., C. and Rosenberg, R., C., *"Anal and simulation of multi Port Systems"*, M.I.T. Pr Cambride, Mass., 1968.

[19] Karnopp, D., C., *"Power-Conserv Transformation"*, Journal of the Franklin Institu Vol, 288, No., 3, Sept. 1969.

[20] Vinke, W., IR., *"Propulsion systems viewed energy transforming and transporting system* Royal Institution of Engineers, Netherlands 197

[21] Chua, L., *"Memristor-the missing circuit elemen* IEEE, Tans. on circuit theory, Sept., 1971.

[22] Rosenberg, R., C. and Karnopp, D., C., *definition of the Bond Graph language"*, Tra ASME, Journal of dynamic systems and contr Sept., 1972.

[23] Rosenberg, R., C., *"Multi-port models mechanics"*, Trans. ASME, Journal of dynam systems, measurements and control, Sept., 1972.

[24] Brown, F., T., *"Lagrangian Bond Graphs". Tran ASME, Journal of dynamic systems, measuremen and control,* Sept., 1972.

[25] Oster, G.F. and Auslander, D.,H., "The memristo a new Bond Graph element, Trans-ASME, Sep 1972.

[26] Martens, H. R. and Bell, A., C., *"A logic Procedure for the construction of Bond Graphs systems modeling, Trans. ASME,* Sept. 1972.

[27] Thoma, J.U, "Introduction to Bond Graphs and the applications.", Pergamon Press, 1975.

[28] Karnopp, D. and Rosenberg, R., *"System dynamic a unified approach"*, John Wiley & Sons, N.Y 1975.

[29] Dransfield, P., *"Hydraulic control systems-desig and analysis of their dynamics, Springer-Verla* Berlin, 1981.

[30] Tylee, J.L., "Computationally convenient stat variables for Bond Graph two-phase accumulators" Trans.ASME, Vol. 105, Sept., 1983.

[31] Tylee, J.L, *"Pseudo Bond Graph representation o PWR Pressurizer dynamics"*, Trans. ASME, Vol 105, Sept., 1983.

[32] Rosenberg, R., C., *"Exploiting Bond Graph causality in Physical system models"*, Trans. ASME Vol. 109, 1987.

[33] Rosenberg, R., C. and Redfield, R. (Ed.), *"Automated modeling for design"*, ASME Winter annual meeting, Chicago, NOV., 1988.